Thin-Walled Structures 192 (2023) 111120

Contents lists available at ScienceDirect

Thin-Walled Structures

journal homepage: www.elsevier.com/locate/tws

Full length article

Finite element modeling of the JCO-E line pipe fabrication process; material properties and collapse pressure prediction

Konstantinos Antoniou [a], Aris G. Stamou [a], Spyros A. Karamanos [a,*], Christos Palagas [b], Athanasios Tazedakis [b], Efthimios Dourdounis [b]

[a] Department of Mechanical Engineering, University of Thessaly, Volos, Greece
[b] Corinth Pipeworks S. A., Thisvi, Greece

ARTICLE INFO

Keywords:
JCO-E pipe
Pipe manufacturing
Yield anisotropy
Welding
Collapse pressure

ABSTRACT

A numerical method for the simulation of the JCO-E pipe fabrication process is presented. The deformation and stresses induced by the manufacturing process, namely the edge crimping, the JCO forming, the LSAW welding, and the expansion (E) operation are calculated utilizing finite element simulation tools. This paper continues a recent work of the authors; it enhances the material model to account for the plate anisotropy, through the development of an in-house material subroutine, and simulates more accurately the welding process. Considering the fabrication parameters of the pipe mill, an X65 line pipe with 26-inch nominal diameter and 0.75-inch nominal thickness is simulated numerically with finite elements. The level of anisotropy is introduced in the model using stress–strain curves obtained from strip specimens, extracted from the steel plate. The predicted material properties of the JCO-E pipe are compared with test results from strip specimens extracted from the produced line pipe. Following the simulation of the fabrication process, and using the same finite element model, the analysis continues so that the mechanical response of the 26-inch-diameter pipe under external pressure is obtained, and its collapse pressure is calculated for different values of the applied expansion. The numerical results show that expansion reduces ovalization and residual stresses in the pipe, and there is an optimum range of expansion strain corresponding to maximum collapse pressure of the JCO-E pipe; beyond that range, the collapse pressure is reduced because of the Bauschinger effect.

1. Introduction

The JCO-E process is a high quality method for producing line pipes with diameter-to-thickness ratio (D/t), which is usually less than 60. These are longitudinal-seam welded line pipes, welded with the submerged-arc welding (SAW) technique, and are candidate for use in both offshore and onshore environment. The first stage of JCO-E process refers to plate edge milling, where the plate edges are trimmed and beveled to accommodate welding in following stage. The plate moves to the crimping press, as shown in Fig. 1a, where the plate edges are formed into circular arcs. Next, the JCO punching press progressively deforms the plate into a round shape (Fig. 1b). Subsequently, the two edges of the deformed plate are mechanically joined and welded using SAW welding machines. The welding process consists of two multi-electrode passes, which perform welding, first on the inside and then on the outside of the pipe (Figs. 1c and 1d, respectively), and the pipe product just after welding is referred to as JCO pipe. After welding, the last forming step, called "expansion", is performed on the JCO pipe through a mechanical expander, as shown in Fig. 1e, to improve and control its geometry. The pipe resulting after unloading from the expansion phase is the final product of this fabrication process, referred to as JCO-E pipe.

The JCO-E manufacturing process is shown schematically in Fig. 2. During the JCO-E forming stages, the steel plate undergoes mainly cold bending, during crimping and JCO punching, and tension, during expansion. This induces significant inelastic deformation in the pipe wall and constitutes an important factor, affecting the ovality of the final line pipe product and its external pressure capacity. The application of expansion allows for the production of pipes with very low initial ovality and residual stresses in the pipe wall. However, experimental results have demonstrated that the collapse pressure of expanded (UOE) pipes can be significantly lower than that of seamless pipes (non-cold-formed, non-expanded pipes) with the same D/t and the same grade steel. The reduction of collapse strength can be as high as 25%–30% and has been demonstrated experimentally in several full-scale collapse test programs on UOE pipes (e.g., [1–3]). The main reason for the reduction of collapse pressure is the large tensile strain induced by the expansion process. In that stage, the pipe wall is subjected to significant hoop tension, well into the inelastic range. As a result, because of

* Corresponding author.
E-mail address: skara@mie.uth.gr (S.A. Karamanos).

https://doi.org/10.1016/j.tws.2023.111120
Received 8 March 2023; Received in revised form 14 June 2023; Accepted 13 August 2023
Available online xxxx

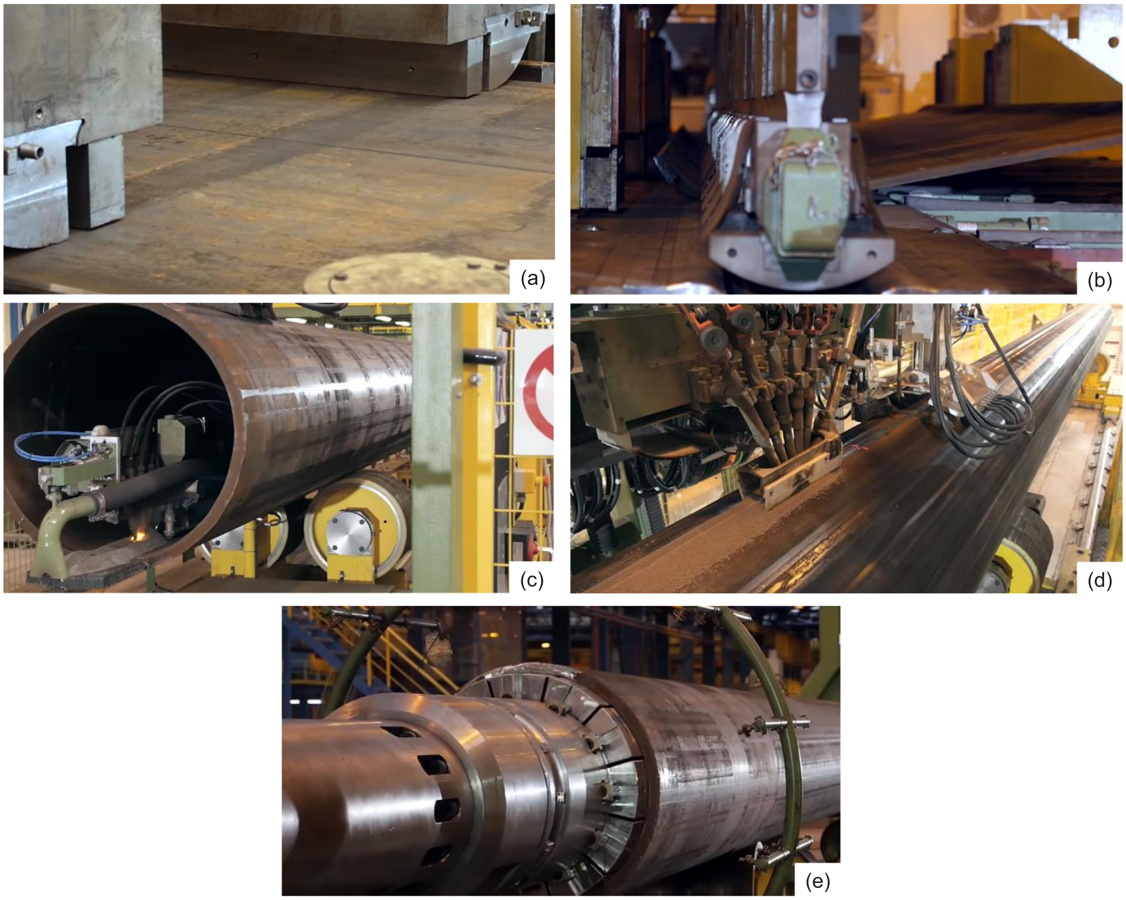

Fig. 1. JCO-E pipe manufacturing process; (a) crimping press, (b) JCO press, (c) inside welding process, (d) outside welding process, (e) mechanical expander [photos provided by Corinth Pipeworks S.A.].

the Bauschinger effect, the compressive strength of the material is reduced, resulting in early yielding of the pipe in compression, and by consequence in a lower value of collapse pressure.

The above issue has been widely recognized as an important factor affecting pipeline structural strength in deep water. The first attempt to address this issue was reported by Kyriakides et al. [4], who adopted a simplified semi-analytical model to quantify the reduction of collapse in a UOE pipe due to cold-forming and expansion. Subsequent numerical studies on UOE pipes have been published by Herynk et al. [5], Toscano et al. [6], Chatzopoulou et al. [7]. More recently, the same issue has been analyzed by Antoniou et al. [8] for the case of JCO-E pipes.

The relevant literature refers primarily on UOE pipes, and the main papers have cited above. On the other hand, the existing literature on JCO-E pipe process and its effect on geometry, material properties and collapse performance of the pipe has received less attention. Chandel et al. [9] simulated the JCO-E manufacturing process and concluded that the radius of the forming tools and dies during line pipe forming play a critical role in forming a geometrically accepted final line pipe. Fan et al. [10] applied a finite element model to simulate the manufacturing of a JCO-E line pipe and presented the consecutive deformation characteristics of its JCO-E forming process. Gao et al. [11] examined numerically the effect of punch displacement on opening width after the JCO steps and found its value that results to an opening width within the accepted range determined by the pipe mill. Kathayat et al. [12] presented examples of numerical studies on JCO-E manufacturing process, and studied, numerically and experimentally, ring collapse showing that coating increases the collapse pressure. Krishnan and Baker [13] examined JCO-E and JCO-C manufacturing processes, and their effect on the collapse pressure of the line pipe. In particular, the JCO-C process consists of uniformly compressing instead of expanding the JCO pipe (final forming step), which is an attempt to overcome the Bauschinger effect on compressive strength. Reichel et al. [14] presented a more detailed investigation on the effect of JCO-C manufacturing process on the material properties of the formed pipe and its collapse pressure.

In the present study, a rigorous model is developed that simulates the JCO-E fabrication process and investigates its effect on the collapse pressure of the pipe, in a unified approach. This paper continues the authors' previous work [8] enhancing the material model to account for yielding anisotropy, quite common in hot-rolled steel plates, using an in-house material subroutine, and simulating more accurately the welding process. This study also compares the numerical results with measurements on the geometric and material properties of the steel plate and the final pipe product obtained from the pipe mill. Using a two-dimensional generalized plane strain model, the crimping phase and the JCO steps are simulated first. Subsequently, the welding process is simulated using an auxiliary three-dimensional solid model, which "communicates" directly with the two-dimensional model; upon completion of the welding simulation, the stress–strain field in the weld area (weld metal and heat-affected zone) obtained from the auxiliary model is transferred to the two-dimensional model, and the analysis continues for simulating the expansion stage. At the end of manufacturing process, geometrical deviations and mechanical properties of the pipe are obtained and the numerical results are compared with available measurements and experimental data, respectively. After unloading from the expansion phase, the fabrication process of the pipe is completed, and the analysis proceeds in its second stage, where

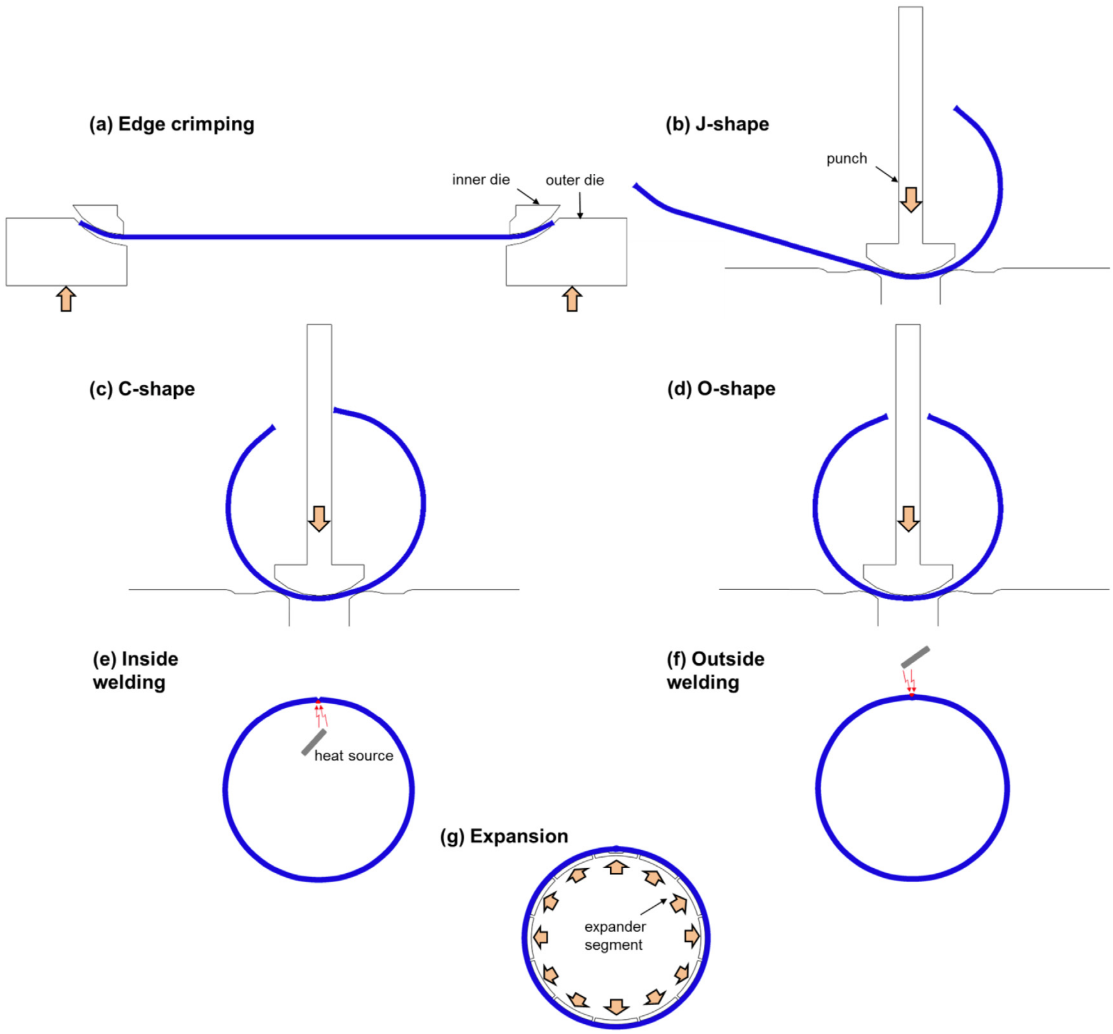

Fig. 2. Schematic representation of the JCO-E manufacturing process; (a) crimping, (b) J-phase, (c) C-phase, (d) O-phase, (e) inside welding, (f) outside welding, (g) Expansion.

the JCO-E pipe is subjected to uniform external pressure, so that its ultimate pressure (collapse) capacity is determined.

The main feature of the present model is the direct correlation between the JCO-E pipe process and its effect on collapse performance under external pressure, a concept also followed in previous publications on UOE pipes [5–7] and by the author's team in [8]. In the present model, the following innovative aspects are considered: (a) the use of a material model that takes into account the anisotropy of steel plate and its implementation in a finite element environment, (b) the development of a three-dimensional auxiliary model for simulating the welding process, (c) the simulation of the entire JCO-E fabrication process and the response under external pressure in a single finite element model, and (d) the comparison of geometric and mechanical properties of the JCO-E pipe obtained from the finite element simulation with actual measurements. The model combines the manufacturing procedure with the structural response in one single analysis. This allows for determining the mechanical properties of the line pipe, and offers a powerful tool for evaluating the collapse performance of the line pipe in deep offshore applications, accounting in a straightforward manner for the residual stresses and the geometric configuration of the line pipe after the fabrication process.

2. Numerical modeling

2.1. Finite element model

A quasi two-dimensional model has been developed to describe the steel plate deformation during the manufacturing process. The model describes the cross-sectional deformation of the steel plate, assuming generalized plane strain conditions. It allows for the simulation of the forming process from the flat plate configuration to the circular shape of the pipe, as well as for the subsequent application of external pressure, in a sequence of analysis steps, towards rigorous calculation of external pressure capacity in a straightforward manner. The use of generalized plane strain conditions, instead of simple plane strain conditions, allows for controlling the out-of-plane deformation and represent the conditions imposed in the pipe mill. The geometry of steel plate, including the geometry of filler material induced in its beveled edges at the welding stage, the geometry of forming dies, the number of punching steps along the plate width, the geometry of the punch, the number and geometry of expander segments, as well as their initial positions and displacements, have been provided by the pipe mill and used as input parameters for finite element model. This model is referred to as the "main model" of the present analysis to distinguish from the "auxiliary model" employed for welding simulation, discussed at a later section.

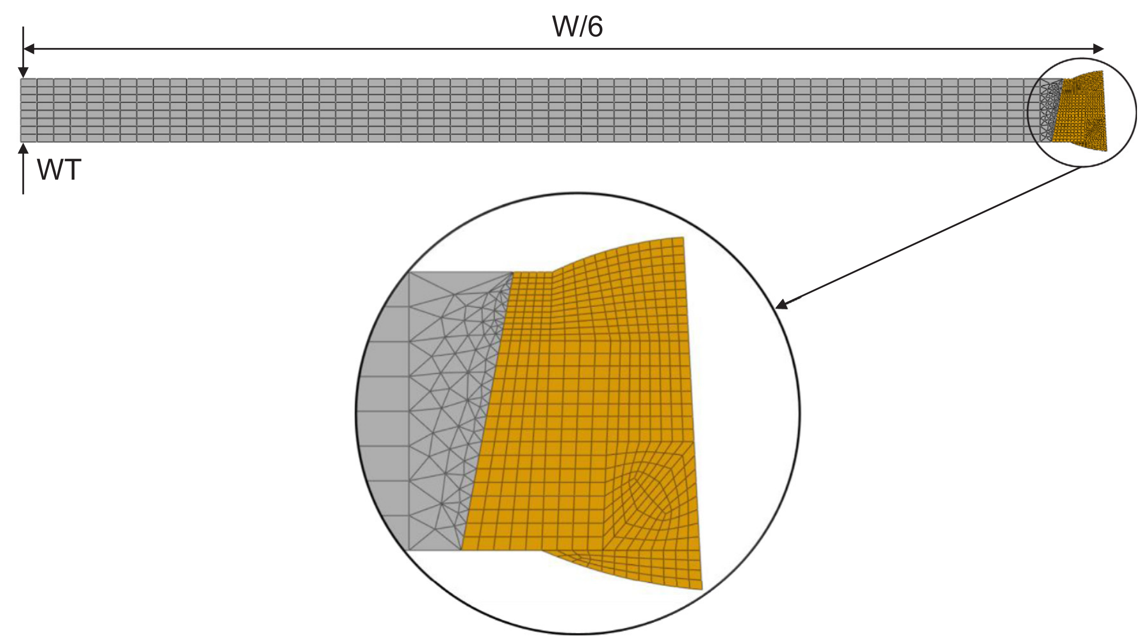

Pipe mill data	Pipe	W (after edge milling) [mm]	WT (mean value) [mm]
Corinth Pipeworks S.A.	26″ OD 0.75″ WT X65	1984	19.44

Fig. 3. A part of the finite element mesh of the steel plate, corresponding to 1/6 of the plate width.

Crimping of the plate edges constitutes an important step of JCO-E manufacturing process that influences the final dimensions near the weld area [9]. During the crimping stage, the inner (top) die is fixed, while the outer (bottom) die is moved upwards forcing the plate edges to obtain the desired bend radius (Fig. 2a). Subsequently, the outer die is retracted and the plate unloads elastically. The analysis proceeds by simulating the JCO forming process (Figs. 2b, 2c, 2d). In this process the plate is subjected to progressively local bending and unloading by applying a series of punching steps along the plate width, while the plate moves from one crimped edge (J-shape) to the other crimped edge (C-shape). The final punching step is applied at the center of the plate, to obtain an O-shape. After the punch is removed, the two plate edges come together, and a "simple" no-slip condition is activated upon contact of the edges.

Subsequently, the welding process is simulated through an auxiliary model that "communicates" directly with the quasi two-dimensional model; the auxiliary model is presented in detail in Section 2.4. At the end of the simulation of welding process, the stresses and the strains in the weld area are transferred to the main analysis model, and the corresponding pipe configuration is referred to as "JCO pipe". Upon completion of welding, the analysis proceeds in simulating the expansion stage. The expander segments (Fig. 2g) are displaced radially in the outward direction forcing the pipe to obtain the desired geometric characteristics. The expander segments are not initially in contact with the internal surface of JCO pipe. When the expander segments start to move radially with the same amount of displacement, the JCO pipe accommodates itself into the new position of the segments. A quasi-circular shape of the pipe is obtained at the stage where all expander segments establish contact with the internal surface of the pipe. Further increase of outward displacement of the expander segments causes pipe expansion and, as a result, the value of pipe diameter approaches its nominal value. After expansion and the corresponding unloading, the as-fabricated product of this manufacturing process is referred to as "JCO-E pipe". Upon reaching the final configuration of JCO-E pipe, and using the same two-dimensional model, uniform external pressure is applied on the external surface of the pipe and a nonlinear analysis is performed using Riks' continuation method. The maximum pressure, reached in this analysis is referred to as "collapse pressure" or "buckling pressure", is obtained, together with the post-buckling response of the pipe.

The model employs analytical rigid surfaces to simulate forming tools and dies. A strict "master–slave" algorithm is used for the contact between forming dies and the steel plate; the master surface refers to the forming dies and the slave surface refers to the steel plate. The contact pairs allow for "finite sliding" between the two surfaces, while contact of the surfaces is assumed to be frictionless. During the JCO steps, it is assumed that no slip occurs between the punching press and the top of the steel plate to avoid relative motion between the two surfaces.

The analysis is implicit and is performed with ABAQUS/Standard. The steel plate is discretized using four-node, reduced-integration generalized plane strain continuum elements, denoted as CPEG4R, which has been proven very efficient for two-dimensional problems, especially in problems involving contact of adjacent surfaces. The density of the finite element mesh has been chosen after a short parametric study. Fig. 3 shows a part of the finite element mesh employed for discretizing both the main part of the plate and the weld area. For the main part of the plate, eight elements are employed through the plate wall thickness (WT), while the size of elements along the plate width (W) is selected to be 1/4 of the plate thickness. The finite element mesh at the weld area is shown with different color in Fig. 3, it corresponds to the size and the number of elements at the weld area of the auxiliary model, and it is quite dense for achieving good accuracy of the welding process simulation.

2.2. Constitutive model

During JCO-E manufacturing process the steel plate material is deformed well into the plastic range and is subjected to reverse plastic

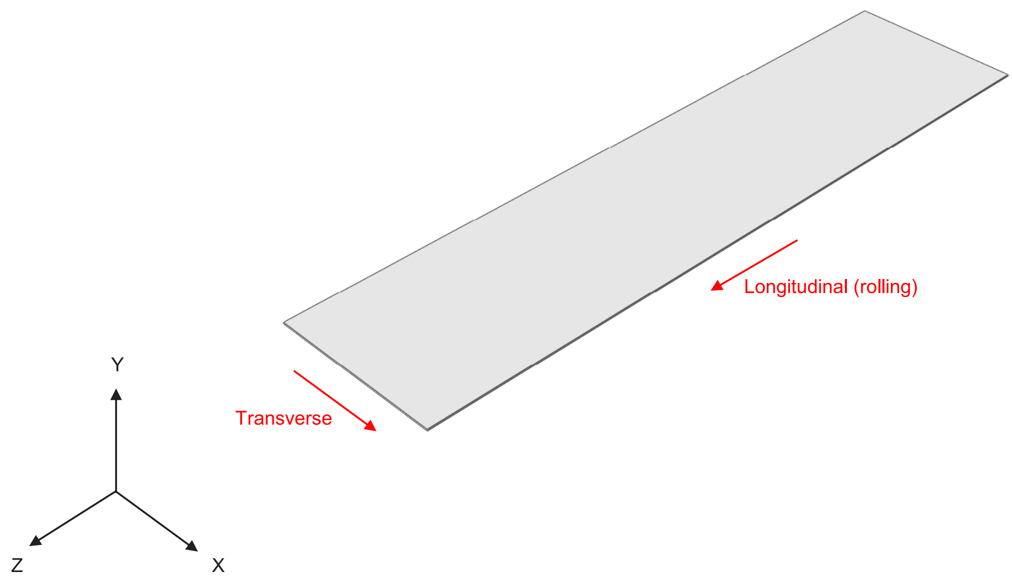

Fig. 4. A schematic of the steel plate showing transverse and longitudinal directions.

loading, where the Bauschinger effect appears. A small anisotropic behavior of the steel plate may also occur at the plastic region due to its rolling production process at the steel mill. This anisotropy implies different yield stresses at different directions of the plate. Therefore, it is important to describe adequately the steel plate material behavior during the elastic–plastic loading conditions considering this anisotropic behavior in order to predict the final properties and the collapse pressure of the JCO-E pipe.

The constitutive model enhances the cyclic plasticity material model employed and implemented by Antoniou et al. [8], and Chatzopoulou et al. [7], which are extended versions of the Armstrong and Frederick model [15]. The enhanced model accounts for anisotropic material behavior, following a formulation similar to that reported in [16], and considers a mixed hardening rule (nonlinear kinematic hardening and isotropic hardening) to describe the changes in size and position of the yield surface due to work material hardening.

The constitutive model is outlined below, and its numerical implementation in a finite element environment is presented in Appendix. Hill's anisotropic yield condition, which accounts for different yield stresses at the three principal directions of the plate using orthotropic plasticity [17] is used. The yield condition is expressed as follows:

$$f_y = \frac{1}{2}(\mathbf{s}-\mathbf{a}) \cdot [\mathbf{N}(\mathbf{s}-\mathbf{a})] - \frac{k^2(\varepsilon_q)}{3} = 0 \tag{1}$$

where $\mathbf{s}$ is the deviatoric stress tensor, $\mathbf{a}$ is the deviatoric back stress tensor, $k(\varepsilon_q)$ is a function of the equivalent plastic strain ε_q that defines the size of the yield surface and $\mathbf{N}$ is a fourth-order tensor of material coefficients representing material anisotropy.

The components of the anisotropy tensor $\mathbf{N}$ are calculated using (a) the tensile yield stresses in the transverse direction $\sigma_{0,x}$, in the through-thickness direction $\sigma_{0,y}$, in the rolling direction $\sigma_{0,z}$, and (b) the yield stresses in pure shear in the (x,y), (y,z), and (x,z) planes denoted as $\sigma_{0,xy}$, $\sigma_{0,yz}$, $\sigma_{0,xz}$, respectively. The transverse and the longitudinal directions of the steel plate with respect to the coordinate system are depicted in Fig. 4. For the purposes of numerical implementation of this model, tensors $\mathbf{s}$ and $\mathbf{a}$ are written in vector form:

$$\begin{aligned} \mathbf{s} &= (s_{xx}, s_{yy}, s_{zz}, s_{xy}, s_{yz}, s_{xz}) \\ \mathbf{a} &= (a_{xx}, a_{yy}, a_{zz}, a_{xy}, a_{yz}, a_{xz}) \end{aligned} \tag{2}$$

and tensor $\mathbf{N}$ is expressed in the following matrix form:

$$\mathbf{N} = \begin{bmatrix} N_1+N_2 & -N_1 & -N_2 & 0 & 0 & 0 \\ -N_1 & N_1+N_3 & -N_3 & 0 & 0 & 0 \\ -N_2 & -N_3 & N_2+N_3 & 0 & 0 & 0 \\ 0 & 0 & 0 & 2N_{xy} & 0 & 0 \\ 0 & 0 & 0 & 0 & 2N_{yz} & 0 \\ 0 & 0 & 0 & 0 & 0 & 2N_{xz} \end{bmatrix} \tag{3}$$

which means that the yield condition in Eq. (1) is written in matrix form as:

$$f_y = \frac{1}{2}(\mathbf{s}-\mathbf{a})^T \cdot [\mathbf{N}(\mathbf{s}-\mathbf{a})] - \frac{k^2(\varepsilon_q)}{3} = 0 \tag{4}$$

The elements of $\mathbf{N}$ are related to the yield stresses in tension and in shear as follows:

$$N_1 = \left(\frac{1}{\sigma_{0,x}^2} + \frac{1}{\sigma_{0,y}^2} - \frac{1}{\sigma_{0,z}^2}\right)\frac{k^2(0)}{3} \tag{5}$$

$$N_2 = \left(\frac{1}{\sigma_{0,z}^2} + \frac{1}{\sigma_{0,x}^2} - \frac{1}{\sigma_{0,y}^2}\right)\frac{k^2(0)}{3} \tag{6}$$

$$N_3 = \left(\frac{1}{\sigma_{0,y}^2} + \frac{1}{\sigma_{0,z}^2} - \frac{1}{\sigma_{0,x}^2}\right)\frac{k^2(0)}{3} \tag{7}$$

$$N_{xy} = \frac{1}{\sigma_{0,xy}^2}\frac{k^2(0)}{3} \tag{8}$$

$$N_{yz} = \frac{1}{\sigma_{0,yz}^2}\frac{k^2(0)}{3} \tag{9}$$

$$N_{xz} = \frac{1}{\sigma_{0,xz}^2}\frac{k^2(0)}{3} \tag{10}$$

It is assumed that the above components are calculated at the initial yielding stage, and do not change during the deformation history. For an isotropic material, Hill's yield criterion results in the well-known von Mises yield criterion. In such a case:

$$\begin{aligned} &\sigma_{0,x} = \sigma_{0,y} = \sigma_{0,z} = \sigma_{0,ij}\sqrt{3} = k \\ &N_1 = N_2 = N_3 = N_{ij}/3 = 1/3 \end{aligned} \tag{11}$$

The isotropic hardening component of the combined hardening rule is expressed in terms of function $k(\varepsilon_q)$, which describes the change in yield surface size in terms of the equivalent plastic strain. Considering the value of $\sigma_{0,x}$ as a reference for the size of the yield surface, defining Q as the maximum change in yield surface size and introducing b as the rate at which the yield surface size changes with plastic straining, the following equation for function $k(\varepsilon_q)$ is adopted, which is also proposed by Lemaitre and Chaboche [18]:

$$k(\varepsilon_q) = \sigma_{0,x} + Q\left(1 - e^{-b\varepsilon_q}\right) \tag{12}$$

Assuming associated plastic flow, from Eq. (1), the plastic strain rate tensor $\dot{\boldsymbol{\varepsilon}}^p$ is expressed as:

$$\dot{\boldsymbol{\varepsilon}}^p = \dot{\lambda}\frac{\partial f_y}{\partial \boldsymbol{\sigma}} = \dot{\lambda}\mathbf{N}(\mathbf{s} - \mathbf{a}) \tag{13}$$

The corresponding equivalent plastic strain rate is defined as:

$$\dot{\varepsilon}_q = \sqrt{\frac{2}{3}\dot{\boldsymbol{\varepsilon}}^p \cdot \left(\mathbf{N}^{-1}\dot{\boldsymbol{\varepsilon}}^p\right)} \tag{14}$$

From Eqs. (13) and (14), it is possible to express the plastic multiplier $\dot{\lambda}$ in terms of $\dot{\varepsilon}_q$:

$$\dot{\lambda} = \frac{3}{2}\frac{\dot{\varepsilon}_q}{k(\varepsilon_q)} \tag{15}$$

The nonlinear kinematic hardening component of the combined hardening rule defines the back stress evolution in the stress space, and it is expressed by the following equation:

$$\dot{\mathbf{a}} = C\left(\varepsilon'_q\right)\dot{\boldsymbol{\varepsilon}}^p - \gamma\mathbf{a}\dot{\varepsilon}_q \tag{16}$$

where γ is a parameter that determines the rate at which the kinematic hardening modulus decreases with increasing plastic deformation and $C\left(\varepsilon'_q\right)$ is a function of the so-called "equivalent cumulative strain" ε'_q, accumulated during a plastic event until unloading. In the primal form of the nonlinear kinematic hardening rule proposed by Armstrong and Frederick [15], the value of $C\left(\varepsilon'_q\right)$ in Eq. (16) is constant. In the present study, function $C\left(\varepsilon'_q\right)$ is defined as follows:

$$C\left(\varepsilon'_q\right) = C_0 + Q_b\left(1 - e^{-c_b\varepsilon'_q}\right) \tag{17}$$

The adoption of function $C\left(\varepsilon'_q\right)$ allows for an efficient description of the Bauschinger effect and the plastic plateau upon initial yielding, and constitutes a key advantage of the present model over the built-in models in commercial software. In Eq. (17), C_0 is the kinematic hardening modulus at initial yielding, Q_b is a parameter representing the maximum change of the initial hardening modulus and c_b is an exponent that controls the rate of this change. For positive values of c_b, negative values of Q_b and increasing plastic deformation, the value of function $C\left(\varepsilon'_q\right)$ decreases exponentially, which is consistent with the Bauschinger effect. The plastic plateau appears upon initial yielding and extends up to a threshold strain value (usually between 0% and 2%, its exact value is determined by experimental data). In the material model, if the equivalent plastic strain is less than this threshold value, the function $C\left(\varepsilon'_q\right)$ and the parameter γ obtain constant small values, representing the very low hardening of the stress plateau.

Enforcing the consistency condition $\dot{f}_y = 0$, using Eqs. (13), (15), (16), and defining $\boldsymbol{\xi} = \mathbf{s} - \mathbf{a}$, one results in the following expression for the equivalent plastic strain rate $\dot{\varepsilon}_q$:

$$\dot{\varepsilon}_q = \frac{1}{\left[\frac{3C\left(\varepsilon'_q\right)}{2k(\varepsilon_q)}(\mathbf{N}\boldsymbol{\xi})\cdot(\mathbf{N}\boldsymbol{\xi}) - \gamma(\mathbf{N}\boldsymbol{\xi})\cdot\mathbf{a} + \frac{2}{3}k(\varepsilon_q)\frac{dk(\varepsilon_q)}{d\varepsilon_q}\right]}(\mathbf{N}\boldsymbol{\xi})\cdot\dot{\mathbf{s}} \tag{18}$$

Furthermore, using the basic elasticity equation $\boldsymbol{\sigma} = \mathbf{D}\boldsymbol{\varepsilon}^e$, where $\mathbf{D}$ is the elastic rigidity tensor, and considering an additive decomposition of the total strain: $\boldsymbol{\varepsilon} = \boldsymbol{\varepsilon}^e + \boldsymbol{\varepsilon}^p$, and the flow rule in Eq. (13) one may write:

$$\dot{\boldsymbol{\sigma}} = \mathbf{D}\dot{\boldsymbol{\varepsilon}} - \dot{\lambda}\mathbf{D}(\mathbf{N}\boldsymbol{\xi}) \tag{19}$$

Tensor $\mathbf{N}\boldsymbol{\xi}$ is deviatoric and, therefore,

$$\mathbf{D}(\mathbf{N}\boldsymbol{\xi}) = 2G\mathbf{N}\boldsymbol{\xi} \tag{20}$$

where G is the shear modulus, and Eq. (19) can be expressed as:

$$\dot{\boldsymbol{\sigma}} = \mathbf{D}\dot{\boldsymbol{\varepsilon}} - \frac{3G}{k(\varepsilon_q)}\dot{\varepsilon}_q\mathbf{N}\boldsymbol{\xi} \tag{21}$$

Finally, the tangent elastoplastic rigidity tensor $\mathbf{D}^{ep}$ is calculated using a standard procedure employed in plasticity models as follows:

$$\mathbf{D}^{ep} = \mathbf{D} - \frac{1}{B}\frac{6G^2}{k(\varepsilon_q)}(\mathbf{N}\boldsymbol{\xi})\otimes(\mathbf{N}\boldsymbol{\xi}) \tag{22}$$

so that $\dot{\boldsymbol{\sigma}} = \mathbf{D}^{ep}\dot{\boldsymbol{\varepsilon}}$. In Eq. (22), symbol $\otimes$ denotes the fourth-order tensor product of two-second order tensors and B is expressed as follows:

$$B = 3\left(\frac{C\left(\varepsilon'_q\right)}{2k(\varepsilon_q)} + \frac{G}{k(\varepsilon_q)}\right)(\mathbf{N}\boldsymbol{\xi})\cdot(\mathbf{N}\boldsymbol{\xi}) - \gamma(\mathbf{N}\boldsymbol{\xi})\cdot\mathbf{a} + \frac{2}{3}k(\varepsilon_q)\frac{dk(\varepsilon_q)}{d\varepsilon_q} \tag{23}$$

The constitutive model is numerically implemented in a user material subroutine (UMAT) of ABAQUS/Standard finite element environment, as described in Appendix.

2.3. Constitutive model calibration

During JCO steps the steel plate is subjected to bending, which involves tension at the outer part of the plate and compression at the inner part of the plate, followed by pure tension during the expansion step. Considering the subsequent application of external pressure, a loading path consisting of a sequence of tension–compression–tension is considered as representative of the stress–strain history, and should be taken into account for the calibration of the model.

Strip specimens are extracted from both the longitudinal and transverse direction of the steel plate and are subjected to tension–compression–tension. These material tests are simulated numerically using a "unit cube" finite element model, i.e. a single "brick" element, with appropriate boundary conditions that represent uniaxial stress conditions. The values of material parameters related to isotropic and kinematic hardening are obtained from cyclic experimental stress–strain curves, considering both longitudinal and transverse direction following a procedure similar to the one described in [19].

2.4. Finite element modeling of the welding process

An auxiliary three-dimensional model is developed for simulating the welding process. The present model uses as input information from half of the pipe cross-section obtained from the main model at the end of O-phase, after the closing of the two plate edges. This information is used for defining the cross-section geometry of the auxiliary three-dimensional model. The auxiliary model represents a pipe length of 100 mm, which is long enough to ensure that the temperature field during the welding passes reaches a steady state. In addition, appropriate symmetry boundary conditions on the X = 0 plane are imposed, as pipe geometry and the welding process are symmetric with respect to the welding line. A thermo-mechanical analysis is performed to simulate the welding process aiming at more realistic description of heat flux compared to the two-dimensional welding simulation, developed and employed in the authors' previous work [8]. Herein, modeling of the welding process is carried out by simulating the two multi-electrode welding passes, with a transient coupled temperature–displacement analysis, which consists of the following steps: (a) first pass (inside welding), (b) cooling to room temperature, (c) second pass (outside welding), and (d) cooling to room temperature. Coupled thermo-mechanical analysis ensures that in each of the above step, the corresponding stresses and strains are also calculated. The pipe is discretized using first-order eight-node, reduced-integration thermally-coupled brick elements, denoted as C3D8RT in ABAQUS/Standard. In

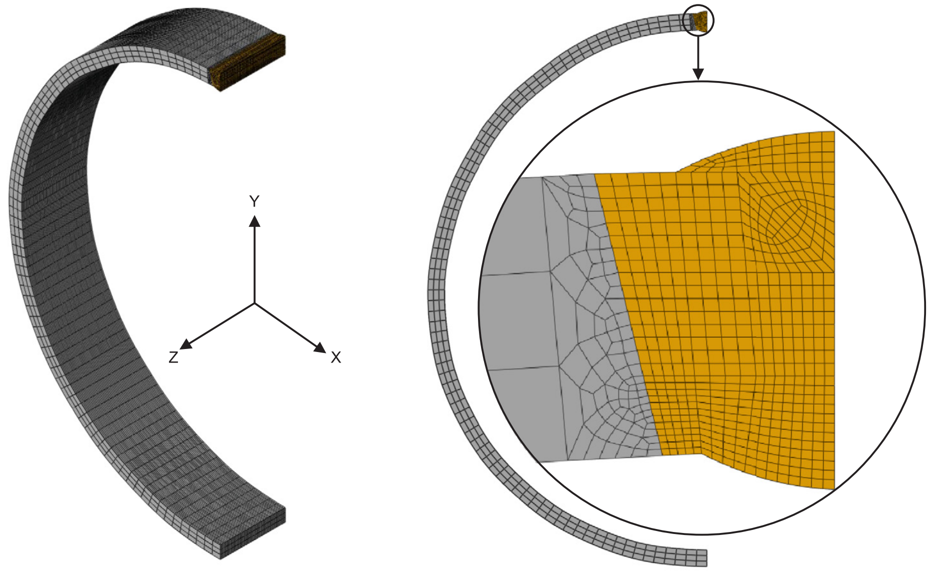

Fig. 5. Finite element mesh of the auxiliary three-dimensional welding model.

the vicinity of the weld area and the heat-affected zone (HAZ), the finite element mesh on the cross-sectional plane of this auxiliary model is depicted with ocher color in Fig. 5, and is identical to the mesh of the two-dimensional main manufacturing model (depicted also with ocher color in Fig. 3). This allows for efficient "communication" between the main model and the auxiliary model; the residual stresses and strains calculated at the weld area under a steady field of temperatures, are the output results of the auxiliary model, which are transferred to the corresponding integration points of the weld area in the main model. Outside this area, the mesh of the auxiliary model is rather coarse, because it is associated with small values of strain and deformation.

In arc welding process, the heat source depends on the welding arc and is quantified by arc power [20]. The power of a single power source is computed by multiplying the arc voltage with the arc current and the efficiency of the welding process; according to ISO/TR 17671-1 document [21], the SAW efficiency can be taken equal to 1. For the SAW process under consideration, the power (heat input)Q, applied during the two multi-electrode welding passes, is considered equal to the sum of the corresponding electrodes power. It is represented in the form of a double-ellipsoid distribution [22], schematically illustrated in Fig. 6, and describes the volumetric heat flux traveling along the welding line. Considering a fixed Cartesian coordinate system $(\mathrm{x,y,z})$ and a moving Cartesian coordinate axis ζ parallel to the z axis, where $\zeta = \mathrm{z} - \mathrm{vt}$, the description of the welding heat source, traveling along welding direction with constant velocity v, includes the front part $(\mathrm{q_f})$ and the rear part $(\mathrm{q_r})$ which are expressed as follows:

$$\begin{aligned} \mathrm{q_f}(\mathrm{x,y},\zeta) &= \frac{6\sqrt{3}\mathrm{f_f}\eta\mathrm{Q}}{\mathrm{abc_f}\pi\sqrt{\pi}}\exp\left(-\frac{3\mathrm{x}^2}{\mathrm{a}^2}-\frac{3\mathrm{y}^2}{\mathrm{b}^2}-\frac{3\zeta^2}{\mathrm{c_f^2}}\right)\forall(\mathrm{x,y},\zeta\geq 0) \\ \mathrm{q_r}(\mathrm{x,y},\zeta) &= \frac{6\sqrt{3}\mathrm{f_r}\eta\mathrm{Q}}{\mathrm{abc_r}\pi\sqrt{\pi}}\exp\left(-\frac{3\mathrm{x}^2}{\mathrm{a}^2}-\frac{3\mathrm{y}^2}{\mathrm{b}^2}-\frac{3\zeta^2}{\mathrm{c_r^2}}\right)\forall(\mathrm{x,y},\zeta< 0) \end{aligned} \tag{24}$$

where η is the welding efficiency, Q is the total heat input, parameters $\mathrm{a,b,c_f,c_r}$ are associated with the heat input, chosen so that the size of the desired melted zone is accurately obtained. The fractions of deposited heat, denoted as $\mathrm{f_f}$ and $\mathrm{f_r}$, are the heat input proportions in the front and rear quadrants, respectively, where $\mathrm{f_f}+\mathrm{f_r}=2$, as proposed by Goldak et al. [22]. During the welding process, the pipe temperature increases due to the thermal load input, but meanwhile, heat losses including natural convection and radiation to the environment from the pipe surfaces are considered in the model.

The auxiliary three-dimensional model employs J_2 flow theory of plasticity with isotropic hardening, where the total strain is decomposed into three components, namely elastic strain, plastic strain, and

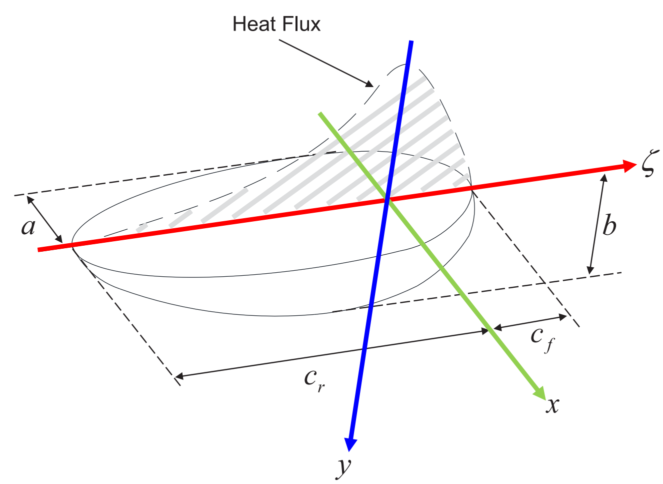

Fig. 6. Schematic representation of the double ellipsoidal heat source.

thermal strain. The corresponding welding residual stresses are affected by the value of thermal expansion [23]. The SAW process is associated with high heat input and high dilution [24] and, as a result, the properties of the filler material are assumed to be same as those of the base metal. During inside welding, the elements corresponding to the not-yet-deposited filler material (outside welding) are considered thermally and mechanically "inactive" (or "invisible"), and are practically non-existent in the model until the outside welding step starts. Thermal "invisibility" means that the material cannot store and conduct heat, which is obtained by setting specific heat and thermal conductivity equal to zero, while mechanical "invisibility" means that mechanical strength and rigidity of the material are negligible, so that these elements are mechanically non-existent and cannot sustain any stress. During the thermo-mechanical analysis, to prevent stress being applied to the melted metal, the thermal expansion coefficient is set to be zero above the melting temperature [25]. Furthermore, temperatures exceeding melting temperature result in stress-free annealing at the steel material, which resets the accumulated plastic strain and the material work-hardening [26]. This stress-free annealing effect is taken into account in the present finite element analysis by setting the accumulated plastic strain equal to zero at a particular element if its temperature reaches or exceeds the steel melting temperature.

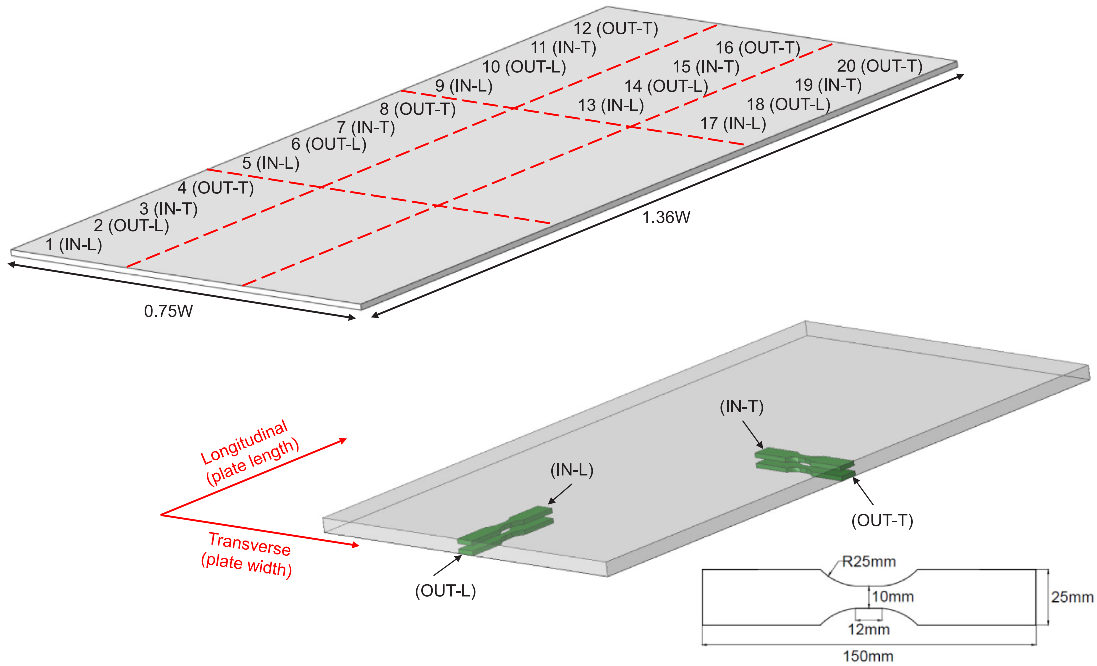

Fig. 7. Adopted notation and position of tested specimens with respect to plate geometry.

3. Results

The methodology for simulating the JCO-E manufacturing process, described in Section 2, is applied to a 26-inch-diameter X65 line pipe with nominal thickness of 19.05 mm, manufactured in Corinth Pipeworks S.A. pipe mill. The line pipe has a nominal diameter-to-thickness (D/t) equal to 34.67 and is candidate for moderate deep offshore applications. Specimens are extracted from the steel plate material and cyclic tests are performed to calibrate the constitutive model. Following the data provided by the pipe mill, including the steel plate characteristics, the forming and the welding parameters, the JCO-E process is simulated by applying fifteen punching steps and using twelve segments in the expander. Geometric characteristics and material properties of the line pipe obtained from the numerical analysis are compared with corresponding measurements from the pipe mill and from pipe material tests, respectively. In the final stage of numerical analysis, uniform external pressure is applied on the external surface of the JCO-E pipe to predict its collapse pressure.

3.1. Geometric parameters

The amount of expansion applied during the last step of the JCO-E manufacturing process, constitutes a key fabrication parameter. It is expressed through the so-called "expansion strain", denoted as ε_E:

$$\varepsilon_E = \frac{C_E - C_W}{C_W} \tag{25}$$

where C_E and C_W are the lengths of pipe circumference after unloading from the expansion phase and the welding stage, respectively. A similar definition of ε_E has also been adopted by the authors in a previous publication [8], and was also used by Herynk et al. [5] and by Chatzopoulou et al. [7]. The value of C_E is measured after removal of the expander and therefore, the expansion strain value ε_E can be considered as a "permanent" expansion strain, where the small "elastic rebound" due to unloading is also taken into account. One should note that the value of ε_E is quite different than the local circumferential strain at a specific location of the pipe. The value of ε_E should be regarded as a "macroscopic" or "global" measure of expansion strain and constitutes a useful parameter to express and quantify the expansion size.

An important geometric parameter with immense influence on pipe collapse under external pressure is cross-sectional ovalization [27,28]. At any stage of pipe deformation, cross-sectional ovalization is expressed through the following parameter:

$$\Delta = \frac{D_{max} - D_{min}}{D_{max} + D_{min}} \tag{26}$$

where D_{max} and D_{min} are the maximum and the minimum outer diameter of the pipe cross-section, respectively, excluding the height of weld bead. Upon completion of the JCO-E manufacturing process, the corresponding value of ovalization parameter in Eq. (26) is referred to as "initial ovalization", or "initial ovality". It is denoted as Δ_o, and expresses pipe cross-section initial ovalization before external pressure is applied.

3.2. Material characterization of the plate and material model calibration

Twenty strip specimens are extracted from both the inner (IN) and the outer (OUT) part of the plate wall, in the longitudinal (L) and the transverse (T) direction, at different locations along the plate length and across the plate width (W), as shown in Fig. 7. The geometry of the specimens follows the provisions of SEP 1240 guideline [29]. Typical experimental results on the tensile response of the steel material at initial yielding (before the application of reverse plastic loading) are presented in Fig. 8; a stress–strain curve from a full-thickness tensile specimen, fabricated according to ISO 6892-1 provisions [30], is also included in the figure for comparison purposes.

The experimental results do not show significant variation in terms of material anisotropy, as depicted in Fig. 9. Furthermore, experimental results from different locations along plate width and length are presented in Fig. 10. The main observation from those tests is that the yield stress of steel plate material in the longitudinal direction is slightly lower compared to the corresponding yield stress in the transverse direction, indicating a low level of anisotropy. Furthermore, comparing the yield stress measured in different locations, the plate material can be considered homogeneous with respect to its tensile properties.

After initial yielding, each coupon is subjected to reverse plastic loading and re-loading, to study the Bauschinger effect. For simulating the steel plate material behavior during elastic–plastic loading conditions, the constitutive model described in Section 2.2 and implemented

Table 1
Material parameters used in modeling the X65 steel material.

E (MPa)	ν	$\sigma_{0,x}$ (MPa)	S_y	S_z	Q (MPa)	b	γ	C_0 (MPa)	Q_b (MPa)	c_b
210,000	0.3	520	0.94	0.94	−30	60	30	10,000	−7,500	150

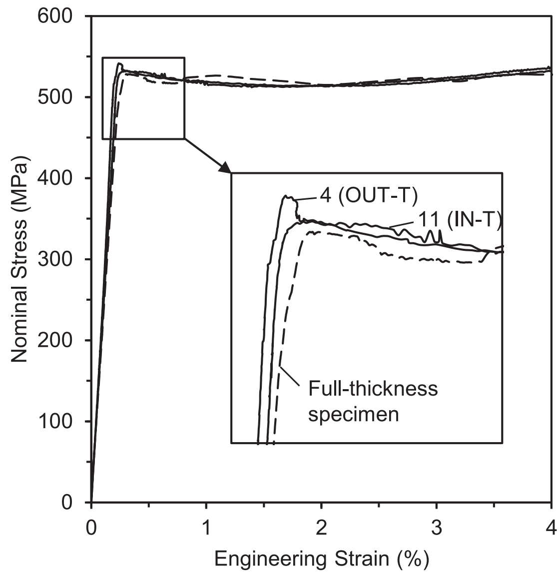

Fig. 8. Measured tensile stress–strain response in the transverse direction of the plate.

(Appendix) in a user material subroutine (UMAT) is used. It is also assumed that the yield stress in the thickness direction ($\sigma_{0,y}$) is equal to the yield stress in the longitudinal direction ($\sigma_{0,z}$). The parameters related to nonlinear kinematic/isotropic hardening are listed in Table 1, and anisotropy is expressed in terms of the anisotropy parameters $S_y = \sigma_{0,y}/\sigma_{0,x}$ and $S_z = \sigma_{0,z}/\sigma_{0,x}$. Fig. 11 shows the stress–strain diagrams obtained from experiments on coupons, extracted from the plate, and the numerical fitting using the material model.

3.3. Modeling of the pipe fabrication process

The crimping and JCO forming steps induce non-uniform stresses in the plate material and the corresponding values of von Mises stress during these stages of fabrication, are shown in Fig. 12. Upon simulation of JCO forming process, the opening width or "gap" between the two plate edges is depicted in Fig. 13 and is very close to the corresponding measurements obtained from pipe mill production. Subsequently, the gap between the two plate edges is closed by applying mechanical loading at the outer surfaces, and upon contact, the two surfaces are not allowed to slide with respect to each other, which is enforced using a "no separation" contact algorithm.

The pipe geometry and the corresponding stress and strain distribution obtained after the closure of the "gap" is used as input for the auxiliary three-dimensional model for the simulation of welding. The auxiliary model communicates directly with the main model. It also considers a pipe length L equal to 100mm. The following welding process parameters, provided by the pipe mill, are used as input in the heat source model: $Q = 3.88$ KJ/mm, $v = 1.91$ m/min for the first (internal) pass and $Q = 5.04$ KJ/mm, $v = 2.00$ m/min for the second (external) pass. The heat source model is implemented using user-defined DFLUX subroutine and the heat source parameters are calibrated using a weld macrograph of the JCO-E pipe, provided by the pipe mill. In this thermomechanical analysis the mechanical properties of X65 steel used in this study (Young's modulus E, Poisson's ratio ν and yield stress $\sigma_{0,x}$) are assumed to depend on temperature according to the data reported in [25]. Based on the work of Nezamdost et al. [31], the melting point of X65 steel is taken equal to 1493 °C and the HAZ refers to a non-melted area of metal, where material has been heated to temperatures in the range of 715–1440 °C. To model the solid–liquid transformation, the latent heat of fusion 2.10 GJ/m^3 is used, a value suggested by Bang et al. [25]. During the simulation of welding process, the heat losses at the free surfaces of the pipe have been modeled by prescribing a convective heat coefficient of 20 W/m^2K, an emissivity of 0.8 and setting the room/ambient temperature at 25 °C.

The distribution of von Mises stress around the pipe cross-section during the second pass (outside welding) is depicted in Fig. 14. The temperature distribution of the selected weld area cross-section, obtained by the finite element analysis at the first and the second pass, is illustrated in Fig. 15. Upon completion of welding process simulation,

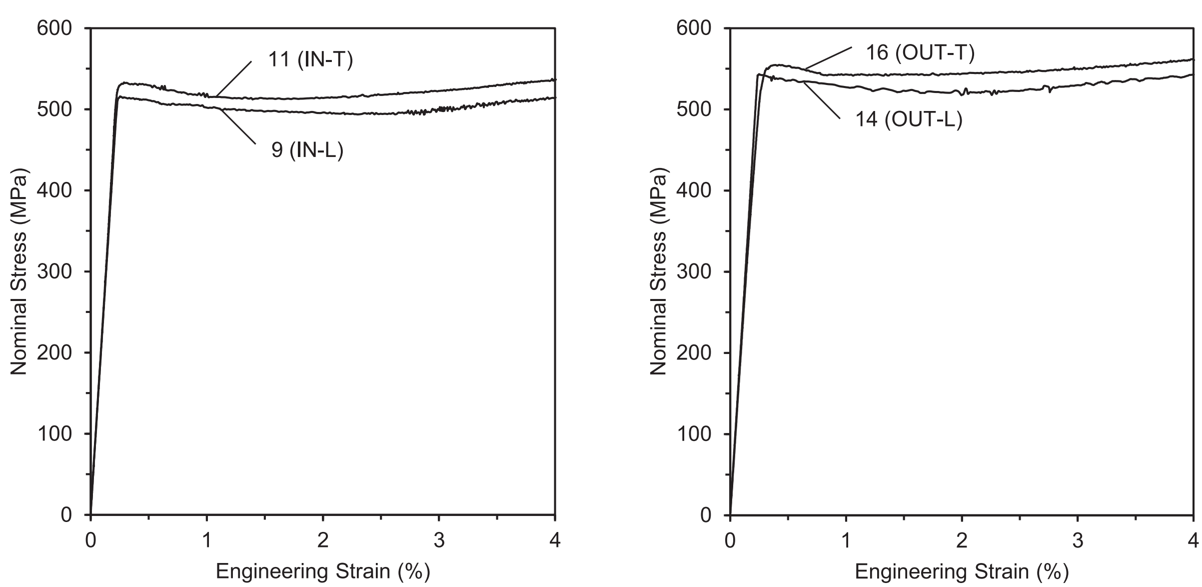

Fig. 9. Stress–strain curves of the steel plate material in the transverse and the longitudinal direction of the plate.

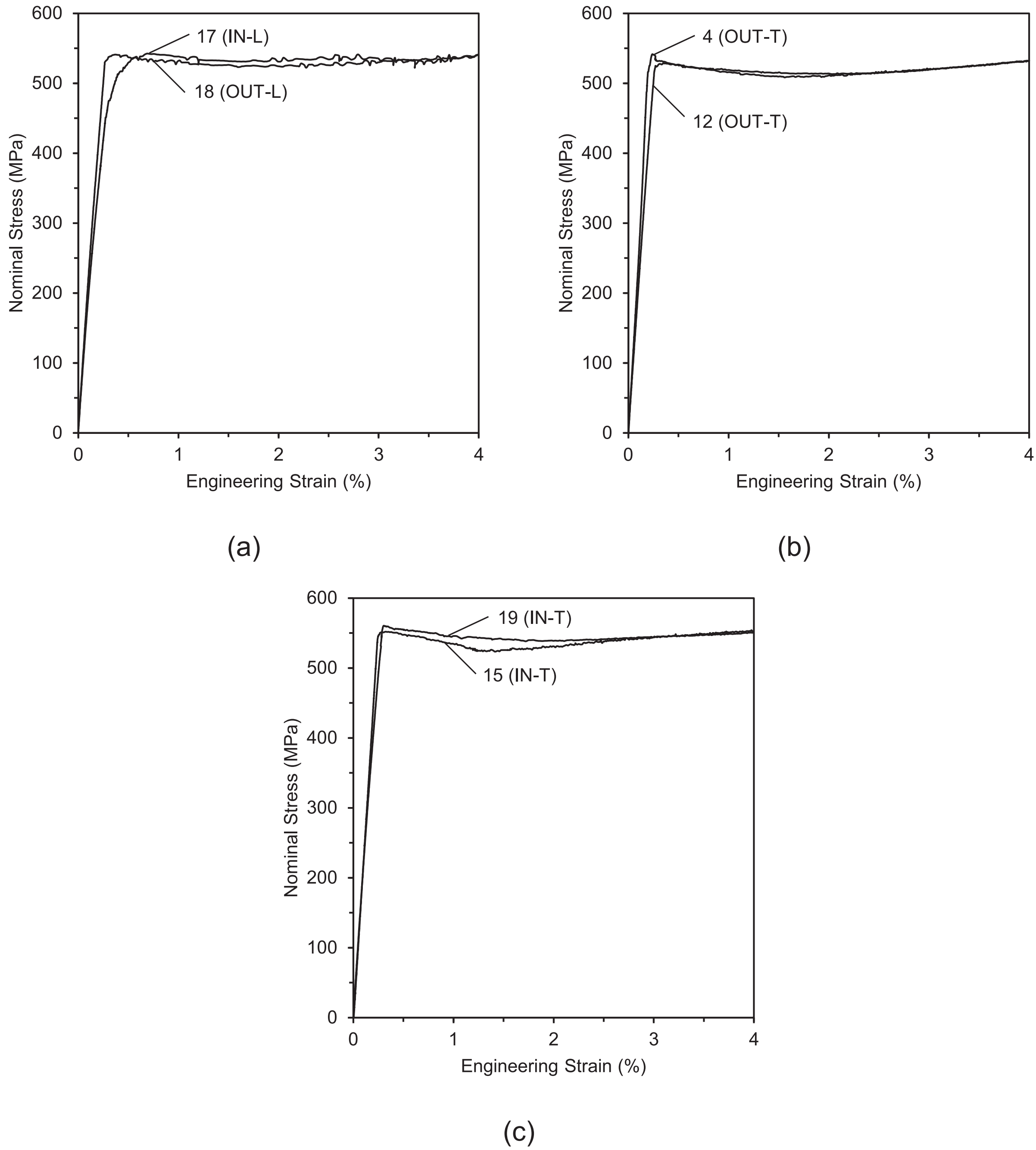

Fig. 10. Stress–strain curves showing the homogeneity of tensile properties in the steel plate; (a) across the thickness of the plate (IN vs OUT), (b) along the plate length, (c) across the plate width.

with the auxiliary analysis, the stresses and strains of the weld cross-section, shown in Fig. 14e with black solid lines, are transferred to the two-dimensional main model, and the simulation of fabrication process continues with the expansion (E) stage.

The distribution of von Mises and hoop stress across the pipe thickness, are shown in Fig. 16 for: (a) the JCO pipe, i.e. when the expander segments are not yet in contact with the inner surface of the pipe, (b) the line pipe expanded at $\varepsilon_E = 1.47\%$ before unloading, and (c) the final JCO-E pipe after removal of the expander segments. The stresses in the JCO pipe increase during pipe expansion, due to the imposed tensile deformation, while after unloading and removal of the expander, there is a significant reduction and homogenization of these stresses, so that the net tension in the pipe wall is zero.

The geometric configuration of the pipe at the end of JCO-E manufacturing process obtained from the present analysis is summarized in Table 2 and is compared with the corresponding measurements provided by the pipe mill. The value of JCO-E pipe diameter (inside or outside) refers to the mean value of the diameter sizes calculated at 30, 60, 90, 120, and 150 degrees from the weld seam. The comparison shows that the computed geometric characteristics of JCO-E pipe are in very good agreement with the pipe mill measurements.

3.4. Mechanical properties of the JCO-E pipe and validation of the model

The JCO-E cold forming process introduces stresses and deformations into the pipe material. As a result, the stress–strain response of the line pipe is substantially modified with respect to the one of the plate material. The mechanical properties of line pipe material at the end of JCO-E process are evaluated experimentally. Strip specimens for

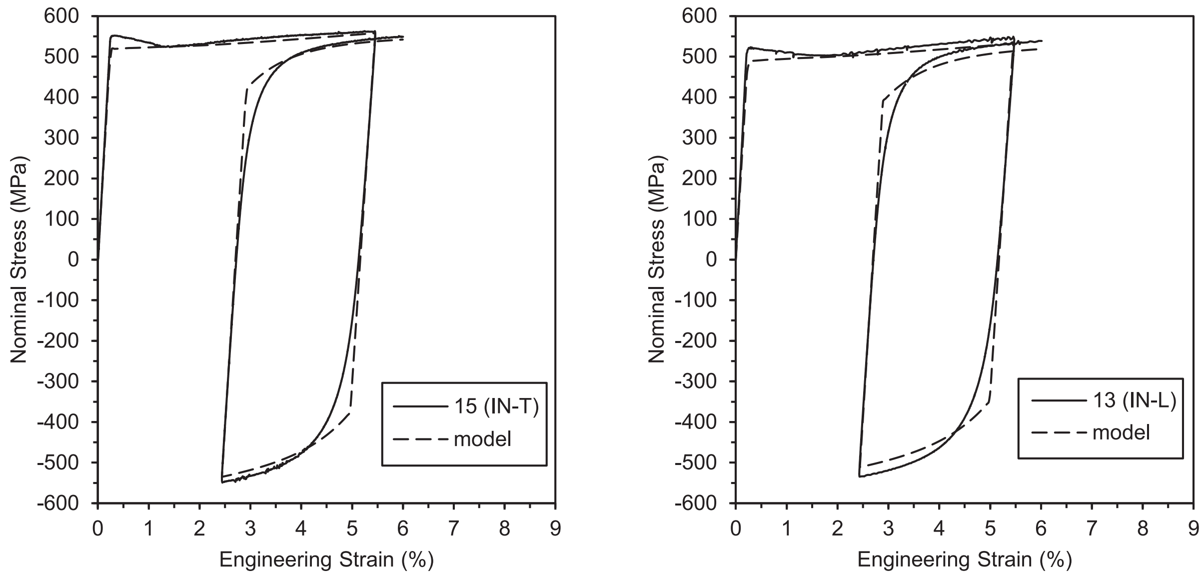

Fig. 11. Stress–strain diagrams, including reverse loading and re-loading from the steel plate experiments, and the corresponding numerical fitting.

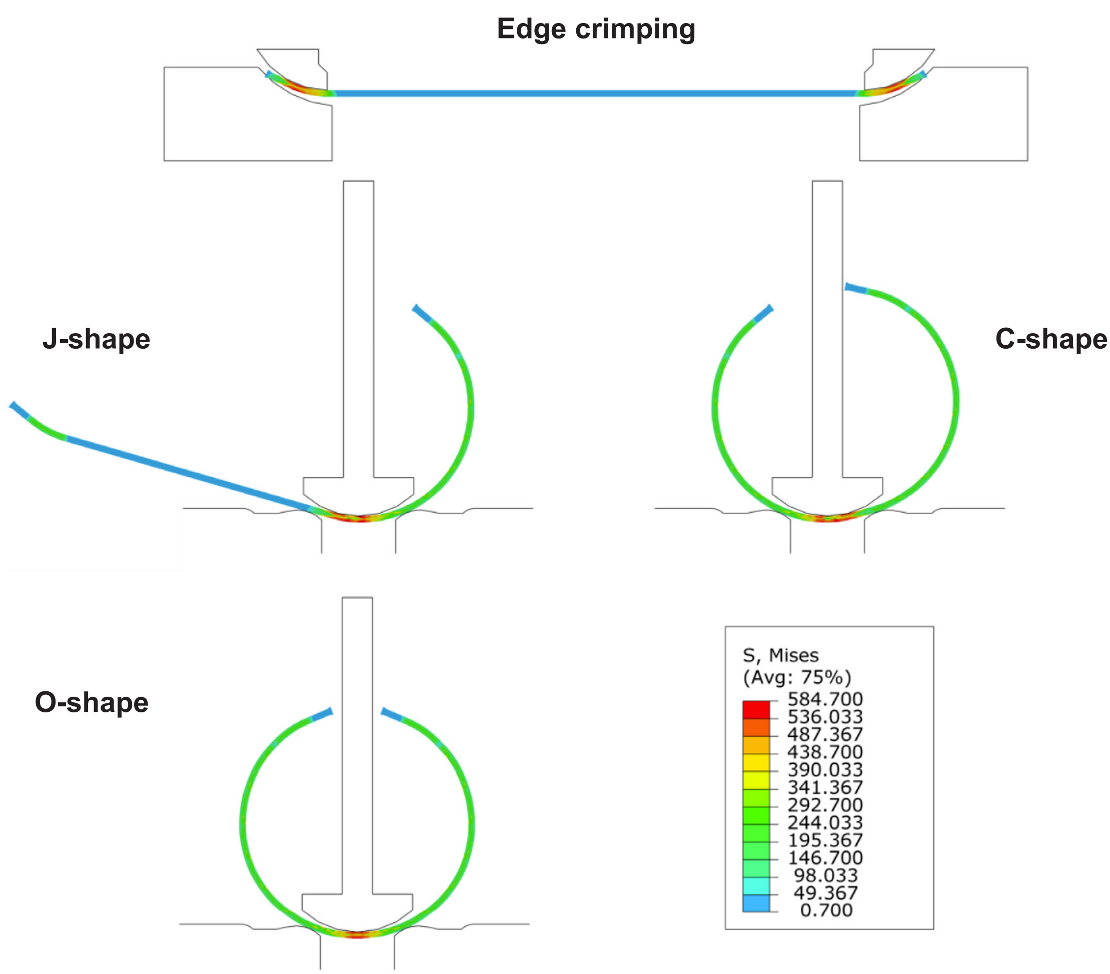

Fig. 12. Consecutive plate configurations during the forming process prior to welding; Von Mises stresses are in MPa.

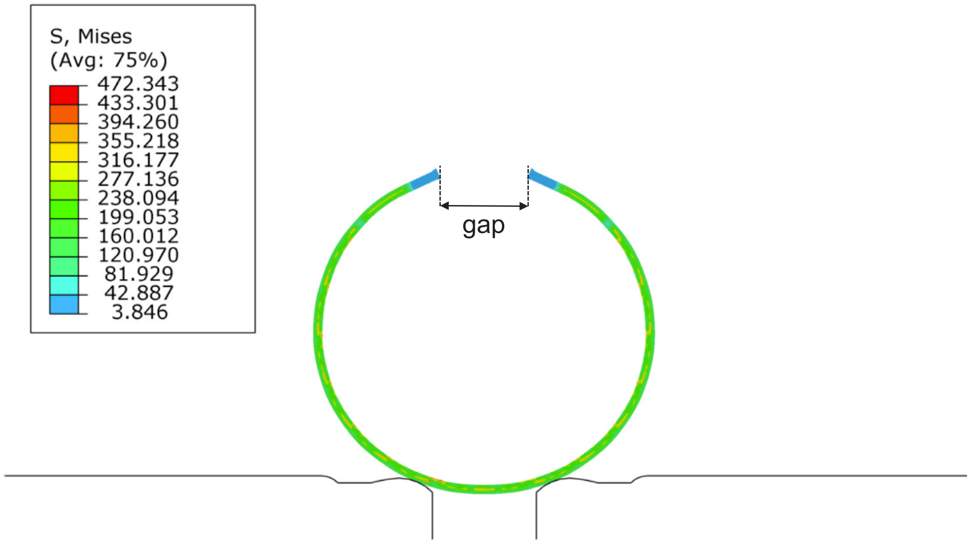

Fig. 13. Plate configuration after the JCO forming; Von Mises stresses are in MPa.

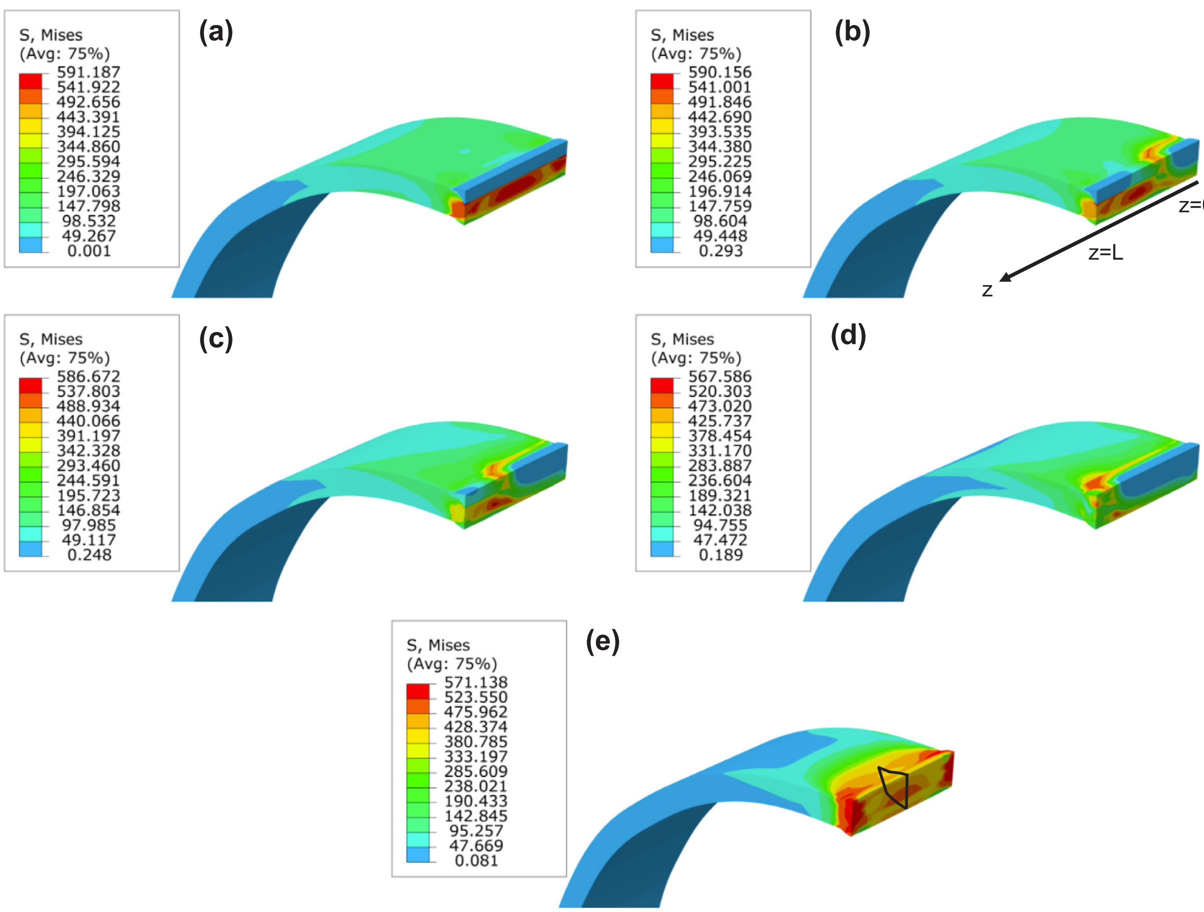

Fig. 14. Von Mises stress distribution [in MPa] in the auxiliary model for different locations of the heat source at outside welding: (a) before outside welding starts, (b) $z = L/4$, (c) $z = L/2$, (d) $z = 3L/4$, and (e) at the end of outside welding.

compressive and tensile testing, according to SEP 1240 guideline, are extracted from the outer (OUT) and the inner (IN) parts of the pipe wall, from both the longitudinal (L) and the transverse (T) direction, as shown in Fig. 17, at 90-degree, 180-degree and 270-degree positions. It should be noted that, the longitudinal direction of the JCO-E pipe coincides always with the longitudinal direction of the initial steel plate, as well as the inner and the outer surface of the pipe coincide always with the corresponding inner and the outer surface of the initial steel plate.

The above experimental testing procedure on strip specimens at the corresponding locations has been simulated numerically considering a "unit cube" finite element model with appropriate boundary conditions. Throughout the finite element simulation of the manufacturing process, the stress–strain history at various locations (integration

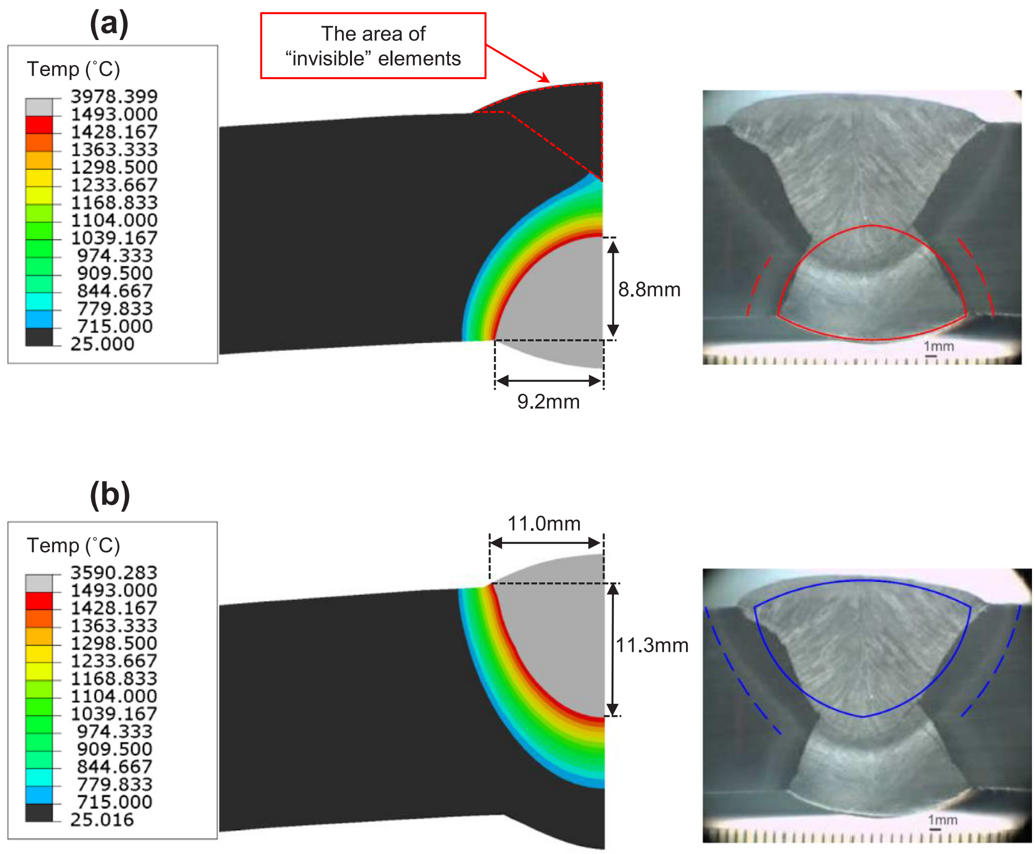

Fig. 15. Comparison between the predicted temperature field of the selected weld area cross-section and the weld macrograph provided by Corinth Pipeworks S.A.; (a) first pass, corresponding to inside welding, and (b) second pass, corresponding to outside welding.

Table 2
Geometric characteristics of the JCO-E pipe.

	Pipe mill measurements	FEM prediction
wall thickness at 90° from the weld seam (mm)	19.17	19.27
wall thickness at 180° from the weld seam (mm)	19.20	19.27
outer diameter of the pipe (mm)	661.70	661.75
inner diameter of the pipe (mm)	623.30	623.20

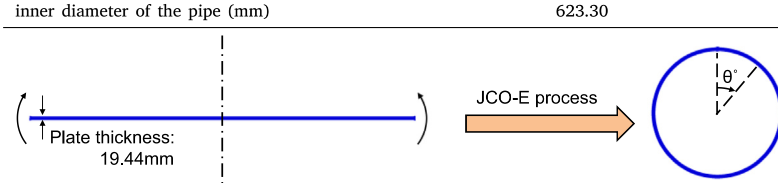

points) around the pipe is recorded. Upon completion of the manufacturing process (after unloading from the expansion phase), the residual stress, strain and state variables at the integration point (IP) of interest are used as initial variables in the “unit cube” model. The above procedure has been performed for eight locations across the thickness of the pipe depicted in Fig. 18 and at 90-degree, 180-degree and 270-degree position. Locations “1, 2, 3, 4” and “5, 6, 7, 8” refer to the inner and the outer half of the pipe wall respectively. In the “unit cube” analysis, an initial step with zero external loading is performed to simulate the strip specimen extraction from the line pipe. At this step, the plastic deformations developed during the manufacturing process are maintained, but the residual stresses are released. Subsequently, uniaxial loading is applied on the “unit cube” in the longitudinal or in the transverse direction, and the corresponding stress–strain curve is obtained.

3.4.1. Compressive response of the pipe material

The compressive stress–strain response of JCO-E pipe material, obtained from the experiments on strip specimens and the numerical predictions at the corresponding location (IP), in the transverse and the longitudinal direction are depicted in Figs. 19 and 20, respectively. In both the longitudinal and the transverse direction, the value of yield strength $R_{t0.5}$ (value of stress at 0.5% strain) at the inner part of pipe wall is higher compared to the $R_{t0.5}$ value at the outer part and this is caused by forming process. During punching, the inner part of the pipe is compressed whereas the outer part is subjected to tension. During expansion the outer part is further loaded in tension well into the hardening region. Therefore when compressed under external pressure it exhibits reverse plastic loading and because of the Bauschinger effect the compressive strength of the pipe material is affected. This compressive strength is lower than that of the inner part. In Fig. 21, the stress–strain curves of the steel plate, presented in Section 3.2, are

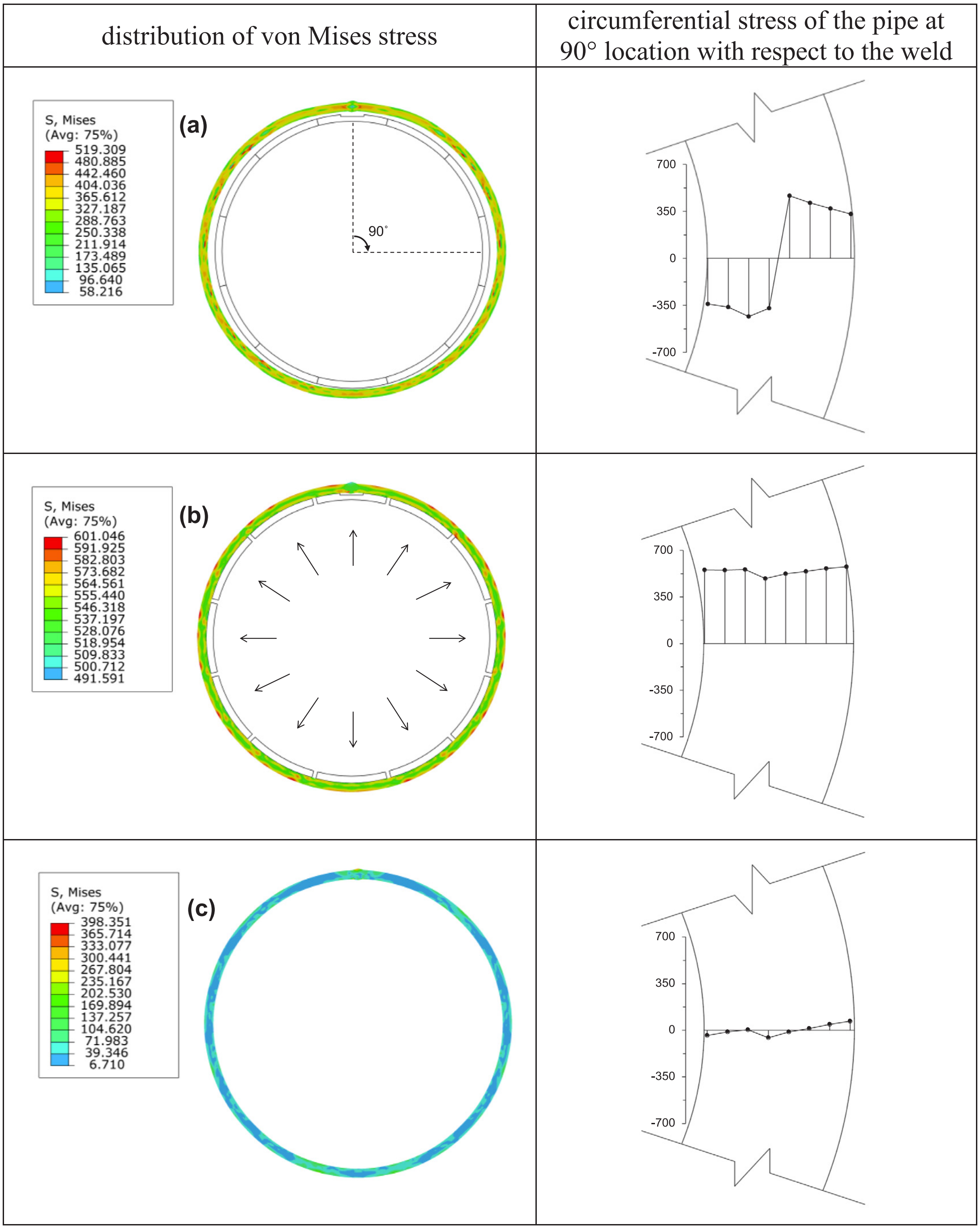

Fig. 16. Distribution of Von Mises stress (left column) and circumferential stress at 90-degree location (right column) in the pipe [in MPa]; (a) at initial position of the expander segments (JCO pipe), (b) at expansion strain of $\varepsilon_E = 1.47\%$ before unloading, (c) after unloading from the expansion phase (JCO-E pipe).

compared with corresponding compressive stress–strain curves of the JCO-E pipe material. The stress–strain curves from Fig. 21 demonstrate that there exists a variation of mechanical properties across the pipe thickness, attributed to the cold forming process.

3.4.2. Tensile response of the pipe material

Measured and predicted tensile stress–strain curves in the transverse direction of JCO-E pipe are depicted in Fig. 22. The measured yield strength $R_{t0.5}$ at the 270-degree position exhibits higher value at the inner part with respect to the corresponding value at the outer part of pipe wall, while for the 90-degree the difference is insignificant. Furthermore, post-yield hardening is smaller with respect to the corresponding one observed in the compressive response (Fig. 19). In the longitudinal direction of the pipe, the tension response of the pipe material at the inner and the outer part of the pipe wall is quite similar to the corresponding compression response presented in Fig. 20.

The comparison between the predicted and measured stress–strain curves (tensile and compressive) is considered satisfactory. In the transverse direction, the measured values of yield strength $R_{t0.5}$ for both compression and tension are summarized in Table 3. In Fig. 23, predicted tensile stress–strain curves at the 90-degree position, are compared with the corresponding predicted curves of the pipe at zero expansion (JCO pipe). Similar calculations are also conducted to obtain compressive stress–strain responses of the JCO and the JCO-E pipe material, which are shown in Fig. 24. The results show that the application

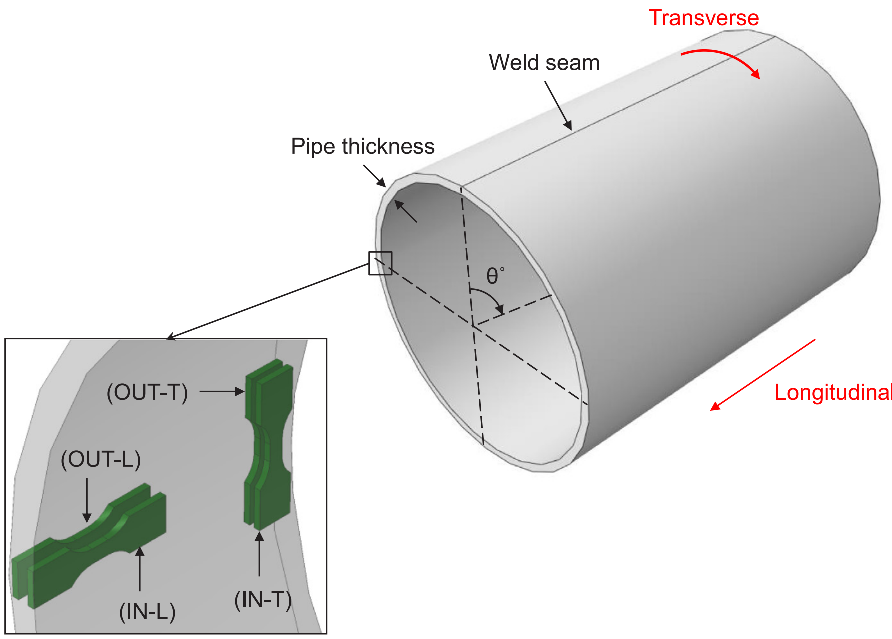

Fig. 17. Location of the strip specimens extracted from the JCO-E pipe.

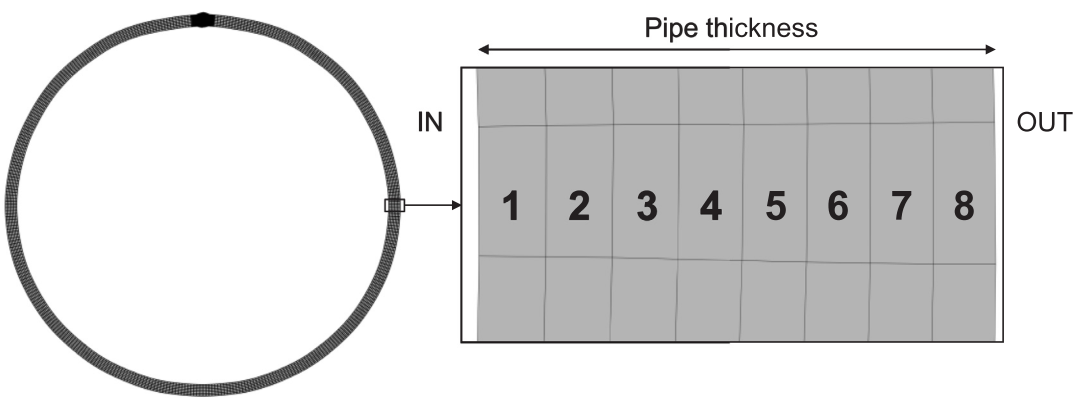

Fig. 18. Numbering of elements at 90-degree position, across the pipe thickness. Similar numbering has been followed in the 180-degree and the 270-degree positions.

Table 3
Measured yield strength $R_{t0.5}$ in the transverse direction of JCO-E pipe.

JCO-E pipe	Yield strength $R_{t0.5}$ (MPa) in transverse (T) direction			
	compression		tension	
	inner (IN)	outer (OUT)	inner (IN)	outer (OUT)
90-degree position	490	421	518	521
180-degree position	495	434	530	506
270-degree position	475	422	550	515
mean value	487	426	533	514

of expansion increases the tensile strength of the pipe material with respect to the plate material, and degrades its compressive strength, an observation consistent with the Bauschinger effect.

3.5. Parametric analysis

3.5.1. Effect of expansion on pipe thickness and residual stresses

During the JCO-E manufacturing process, the plate is subjected to circumferential tension and, as a result, the thickness of the pipe at the end of the process is different than the initial plate thickness. A parametric study is conducted to examine the effect of expansion on pipe thickness. Both the average thickness of the pipe $t_{average}$ and the expansion strain ε_E refer to the stage after unloading from the expansion phase. The value of $t_{average}$, is calculated from the thickness values at 90-degree, 180-degree and 270-degree positions, and is presented in Fig. 25 with respect to the ε_E value. The numerical results show that the $t_{average}$ value decreases with increasing values of ε_E in a quasi linear manner. For zero expansion (JCO pipe), the average thickness is equal to 19.38 mm, a value very close to the steel plate thickness. As the expansion level increases, the wall thickness of the pipe is reduced mainly due to the net tension induced in the pipe wall. For expansion strain $\varepsilon_E = 2.08\%$, the average thickness is equal to 19.21 mm, which is an 1.18% reduction with respect to the initial plate thickness (19.44 mm).

The residual stresses of JCO-E pipe in the circumferential direction at the 90-degree and 180-degree positions are presented in Figs. 26 and 27, respectively. In those figures, $\sigma_{c,max}$ denotes the maximum value of the circumferential stress and the yield stress value σ_y is equal to 523 MPa, which is the mean value of hoop yield strength $R_{t0.5}$ measured in the tensile coupon tests. The numerical results in Figs. 26 and 27 demonstrate clearly that the increase of expansion reduces the residual stresses of the JCO-E pipe, which has also been shown in Fig. 16.

3.5.2. Effect of expansion on external pressure capacity

Apart from simulating the JCO-E manufacturing process and predicting line pipe properties, the finite element model is capable of

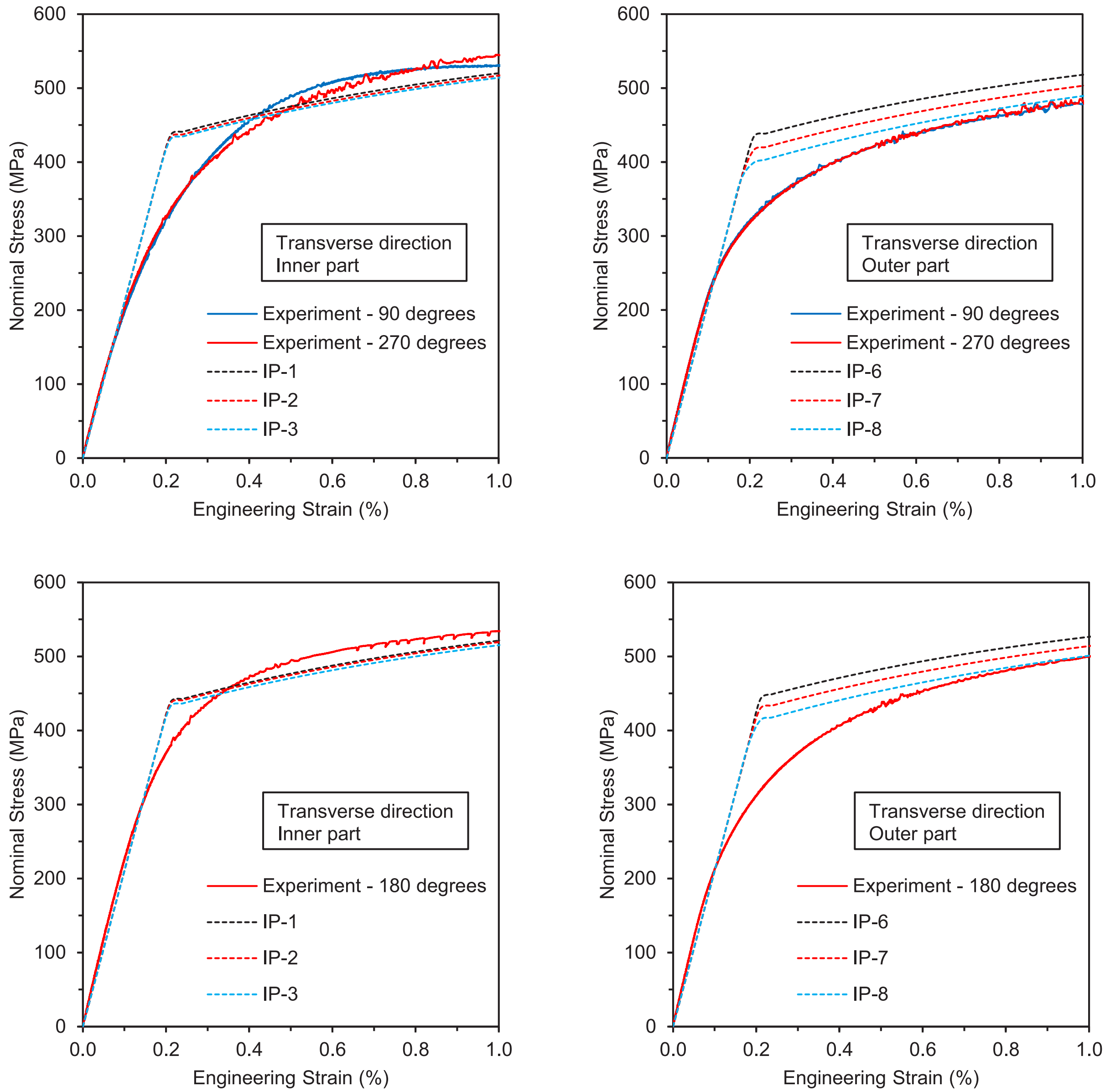

Fig. 19. Measured and predicted compressive stress–strain response in the transverse direction of the pipe.

predicting the influence of manufacturing process on structural performance. Towards this purpose, the analysis continues beyond manufacturing and uniform external pressure is applied on the JCO-E pipe to calculate its collapse pressure and post-buckling response.

A numerical study is performed to examine the effects of ε_E value on initial ovalization Δ_o and the collapse of the pipe. Fig. 28 presents the predicted collapse pressure P_{CO} and the corresponding initial ovalization parameter Δ_o in terms of the applied (permanent) expansion strain ε_E. For a small value of expansion strain ($\varepsilon_E = 0.10\%$), the corresponding initial ovalization is $\Delta_o = 0.14\%$, and the corresponding collapse pressure P_{CO} is equal to 11.30 MPa. With increasing expansion, the value of Δ_o drops sharply, causing a significant increase of P_{CO}. More specifically, the value of Δ_o decreases rapidly to a value of approximately 0.03% up to ε_E equal to about 0.5%. Upon additional outward movement of the expander segments ($\varepsilon_E > 0.5\%$), the value of Δ_o remains nearly constant at 0.03%. For ε_E values between 0.45% and 1.15%, the collapse pressure remains nearly constant, and this range of ε_E constitutes the optimum expansion range for the line pipe under consideration, as shown in Fig. 28. The maximum collapse pressure of 12.35 MPa is obtained at $\varepsilon_E = 0.50\%$. Increasing the expansion strain beyond the value of $\varepsilon_E = 1.15\%$, the corresponding collapse pressure decreases. Under those large expansion strains, the degradation of compressive strength in the pipe material, because of the Bauschinger effect, overshadows the improvement of initial ovality and the minimization of residual stresses, and leads to reduction of collapse pressure. Application of external pressure results in a progressive increase of cross-sectional ovalization, from Δ_o to a current value Δ. In addition, the deformed shapes of the JCO-E pipe for $\varepsilon_E = 0.50\%$, at collapse and at post-buckling, are shown in Fig. 29.

In an attempt to interpret the influence of JCO-E fabrication process on the collapse pressure of the as-fabricated pipe product, a "fictitious" pipe is considered, and is subjected to uniform external pressure under plane strain conditions. This fictitious pipe refers to a two-dimensional pipe model, which has zero residual stresses and strains (before the application of external pressure), so that the deformation history during its fabrication process is neglected. The elastic–plastic material behavior of the fictitious pipe is assumed to be described by the material parameters of the plate material (Table 1). The cross-section of the fictitious pipe is initially oval, with ovalization amplitude equal to $\Delta_o = 0.03\%$ (i.e., the minimum ovality of the JCO-E pipe), thickness

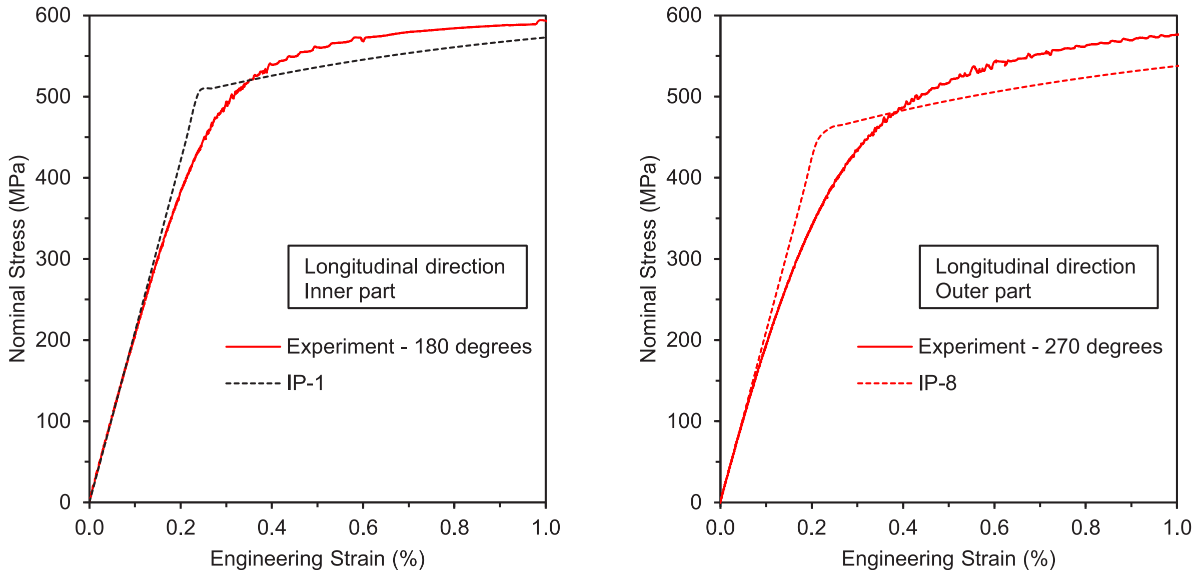

Fig. 20. Measured and predicted compressive stress–strain response in the longitudinal direction of the pipe.

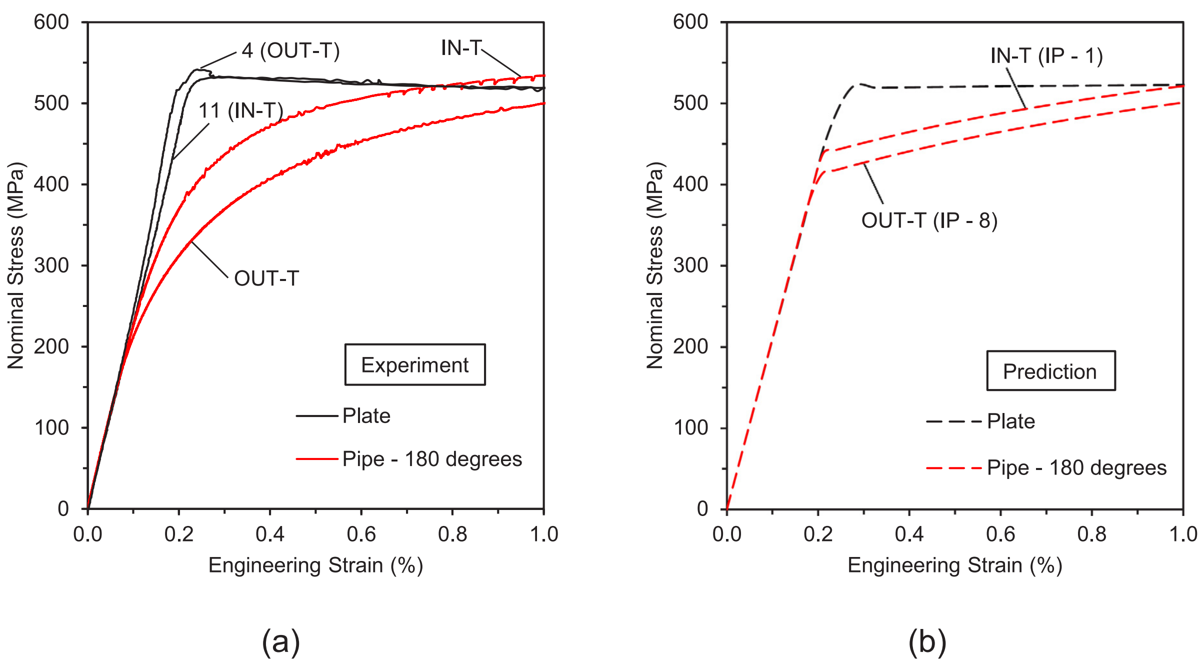

Fig. 21. Transverse stress–strain response of the plate material in comparison with the JCO-E pipe material tested in compression, obtained from (a) experiments and (b) numerical model.

equal to the plate thickness, (t = 19.44 mm), and outer diameter equal to the nominal outer diameter of JCO-E pipe (26 inches). The collapse pressure of fictitious pipe is 12.73 MPa, which compares quite well with the maximum collapse pressure of JCO-E (12.35 MPa) in Fig. 28. Therefore, if an "optimum expansion" is applied on the JCO-E pipe, the effect of the fabrication process on collapse pressure can be minimized.

The maximum collapse pressure of the JCO-E pipe computed numerically is also compared with the corresponding predictions of DNV-ST-F101 [32] and API 1111 [33] standards, which are widely used in offshore pipeline design. The DNV-ST-F101 formula assumes an initial ovality parameter Δ_o equal to 0.25%, and for the purposes of the present calculation a fabrication factor α_{fab} = 0.85 is considered. This value of α_{fab} refers to JCO-E pipes and accounts for the detrimental effects of cold forming process on the collapse resistance of line pipe. The material and geometric parameters considered in the corresponding equations and the predictions from the two standards are shown in Table 4. In order to conduct a fair comparison with the finite element results, safety factors/margins suggested by the standards are not taken into account. The collapse pressure predictions from [32,33] are approximately 16% lower with respect to the maximum collapse pressure obtained from the numerical analysis results, which is a satisfactory yet conservative result.

3.5.3. Effect of welding process on collapse pressure

The effect of welding process on the external pressure resistance of the JCO-E pipe is also examined. An analysis of the cold bending JCO-E process similar to the one described in Section 2 is performed using the forming data provided by the pipe mill, but excluding the thermo-mechanical simulation of the welding process described in Section 2.4.

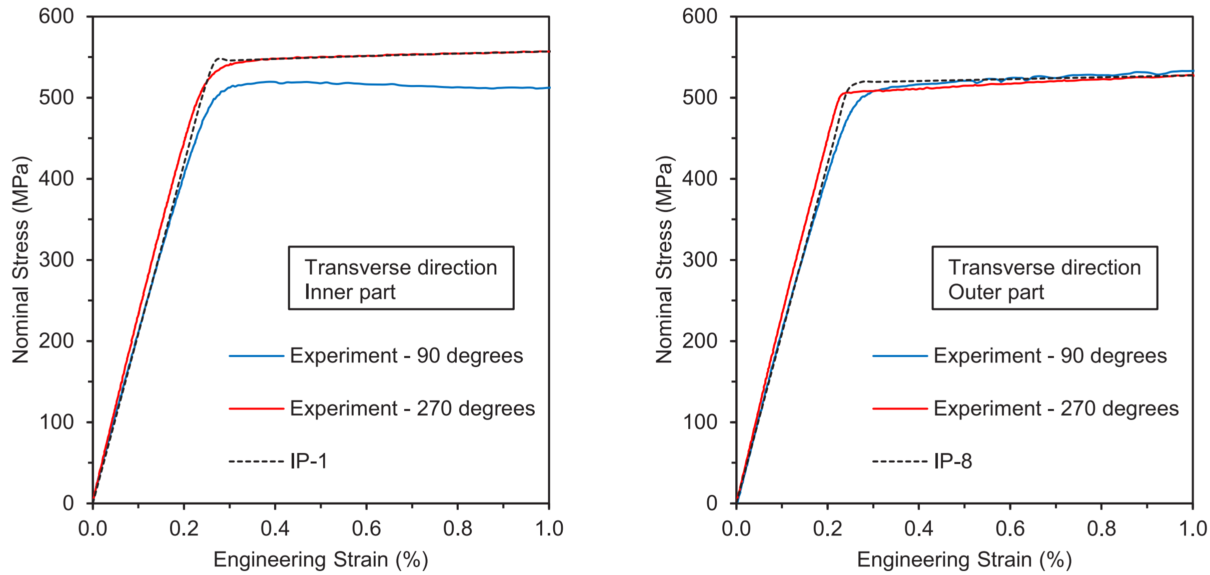

Fig. 22. Measured and predicted tensile stress–strain response in the transverse direction of the pipe.

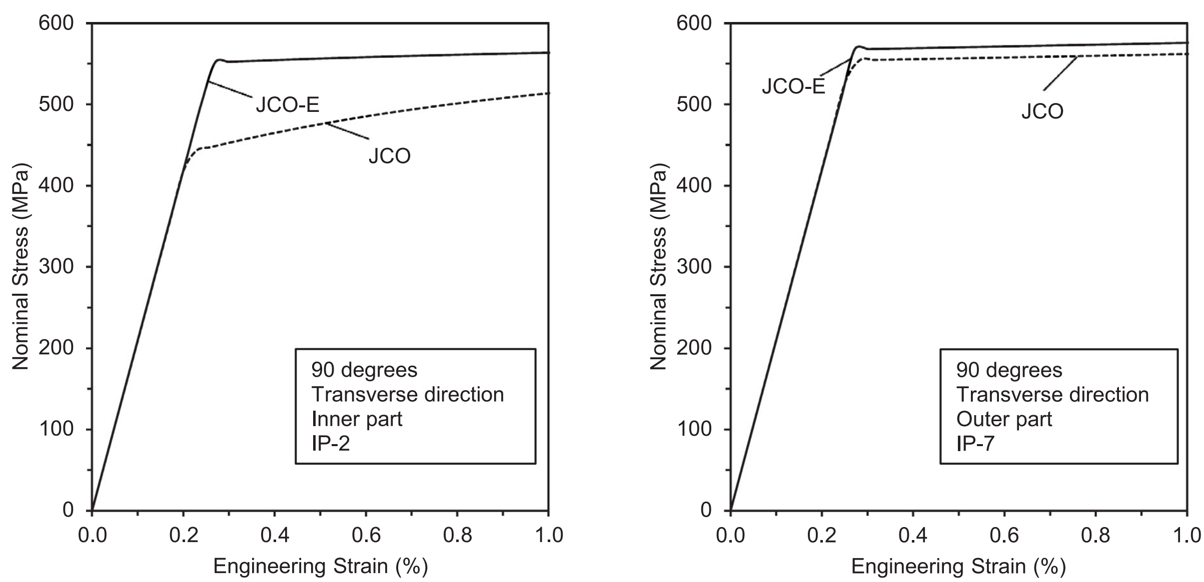

Fig. 23. Predicted tensile stress–strain response of the JCO pipe (non-expanded) and the JCO-E pipe.

Table 4
Pipe collapse pressure according to DNV and API design equations.

JCO-E pipe parameters	Collapse pressure equation	
	DNV-ST-F101	API 1111
• Elastic material parameters: E=210 GPa, $\nu = 0.3$ • Assumptions for DNV-ST-F101 calculations: $\alpha_{fab} = 0.85$, $O_0 = 2\Delta_o = 0.5\%$ • Yield strength $R_{t0.5}$: 523 MPa (mean value measured in the tensile experiments of coupons obtained from the transverse direction of the pipe) • Pipe wall thickness: 19.19 mm (mean value measured in the pipe mill) • Outer pipe diameter (measured in the pipe mill and shown in Table 2): 661.7 mm	10.33 MPa	10.55 MPa

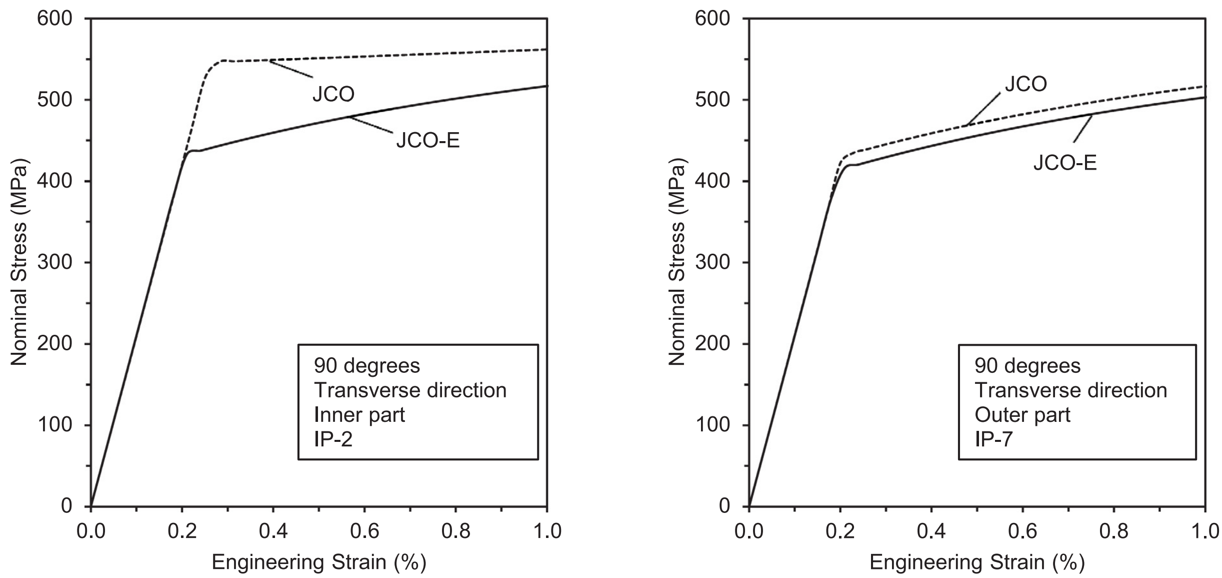

Fig. 24. Predicted compressive stress–strain response of the JCO pipe (non-expanded) and the JCO-E pipe.

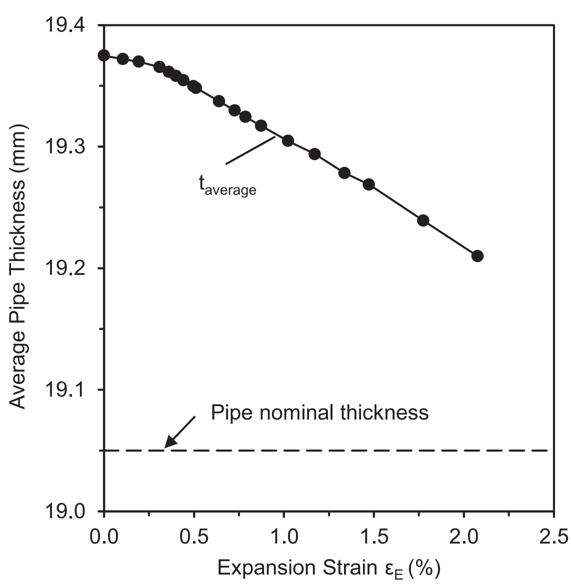

Fig. 25. Average pipe thickness $t_{average}$ in terms of expansion strain.

In this study the mechanical properties of X65 steel (E, ν and $\sigma_{0,x}$) are considered independent of temperature. This analysis is referred to as "mechanical analysis" and involves a purely mechanical connection between the two edges of the pipe after the O-phase, using appropriate kinematic conditions. The results from this mechanical analysis, show that the value of collapse pressure P_{CO} is greater by only 0.14 MPa than the corresponding value obtained by the full thermo-mechanical model (1.17% difference). This is a clear indication that the welding process has a negligible effect on collapse pressure of the JCO-E pipe, because its effects are limited to a small part of the pipe cross-section at the weld area.

3.5.4. Effect of anisotropy on collapse pressure

Considering the "mechanical analysis" described above, a short parametric study is conducted to examine the effect of anisotropy on the collapse pressure. The assumed anisotropic parameters correspond to five cases of steel plate material properties. For each case, the calculated initial ovalization Δ_o and the normalized value of collapse pressure P_{CO}/P_y are listed in Table 5, and correspond to expansion strain $\varepsilon_E = 0.50\%$.

Table 5
Effect of anisotropy on collapse pressure.

Steel plate ($\sigma_{0,x} = 520$ MPa)	JCO-E pipe	
anisotropy constants	P_{CO}/P_y	Initial ovalization Δ_0 (%)
$S_y = S_z = 0.94$	0.415	0.032
$S_y = S_z = 0.90$	0.415	0.026
$S_y = S_z = 0.85$	0.414	0.025
$S_y = 1.00$, $S_z = 0.94$	0.416	0.030
$S_y = S_z = 1.00$	0.416	0.024

The first case corresponds to the anisotropy measured from the tensile coupon tests of the plate, used throughout the present work. In this case, it is also assumed that the yield stress in the thickness direction is equal to the yield stress in the longitudinal direction. The additional cases of material anisotropy in Table 5 consider the same JCO-E process and show that anisotropy of the steel plate, within the range indicated by the material tests, have a slight influence on the value of collapse pressure. This result is attributed to the relative large value of diameter-to-thickness ratio (D/t = 34.67) and is consistent with numerical studies on the influence of residual stresses reported in [27,28]. In addition, the corresponding value of initial ovality (Δ_o) at the end of the fabrication process is practically unaffected by the value of anisotropy. This implies that the JCO-E forming process of the line pipe under consideration can be modeled with reasonable accuracy using a cyclic plasticity model with isotropic (von Mises) yield function, employed in previous publications [7,8].

4. Conclusions

A generalized plane strain finite element model is developed that describes the entire deformation history of the pipe during the JCO-E manufacturing process, from the initial steel plate configuration to the final JCO-E pipe product. The model predicts the response of the pipe under uniform external pressure and calculates its collapse pressure, accounting rigorously for the effects of pipe fabrication on the material and geometric properties of the final pipe product. In this

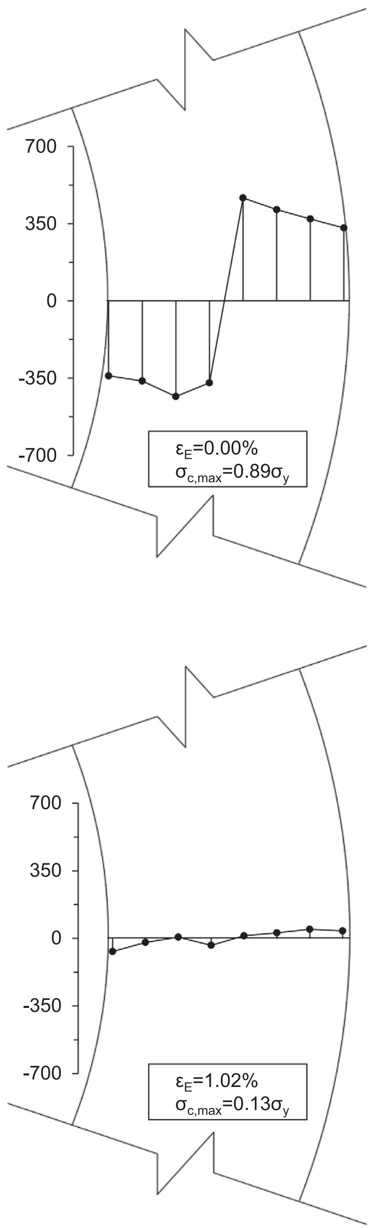

Fig. 26. Circumferential residual stress distribution [in MPa] across the thickness of the JCO-E pipe at 90-degree position, for different values of expansion strain. The first picture (top-left) refers to JCO pipe (no expansion).

model, the welding process is also simulated using an auxiliary thermo-mechanical analysis model. For simulating the steel plate material behavior under the cold forming conditions and accounting for possible material anisotropy, an anisotropic material model is developed and implemented as a user material subroutine in the finite element model.

The finite element model is employed to simulate the fabrication and collapse resistance of an JCO-E X65 steel pipe, with nominal diameter of 26-inch and nominal wall thickness 0.75-inch (19.05 mm), adopting the manufacturing parameters provided by the pipe mill. Strip specimens are extracted from the raw material (steel plate) and subjected to cyclic loading, and the stress–strain curves are used to calibrate the anisotropic material model. From these tests, the anisotropy ratio on the yield stress is found equal to 0.94, which implies that plate anisotropy is rather small. The geometry of the simulated JCO-E pipe is also found to compare well with pipe mill measurements. Strip specimens are also extracted from the final JCO-E pipe product, in the transverse and the longitudinal direction, to measure their compressive and tensile response and strength. Overall, the comparison between those experimental results and the corresponding numerical predictions has been very satisfactory, verifying the influence of the Bauschinger effect.

The effect of expansion on pipe geometry, pipe material properties, residual stresses and pipe collapse strength has been investigated. The model predictions show that the reduction of JCO pipe thickness is quasi-linear with respect to increasing expansion level. Expansion increases the tensile strength of the pipe material in transverse direction due to strain hardening, but reduces the residual stresses and the initial ovalization of pipe. Furthermore, expansion is beneficial for the collapse resistance of the pipe up to a relatively small level, and there exists an optimum expansion range for achieving maximum collapse

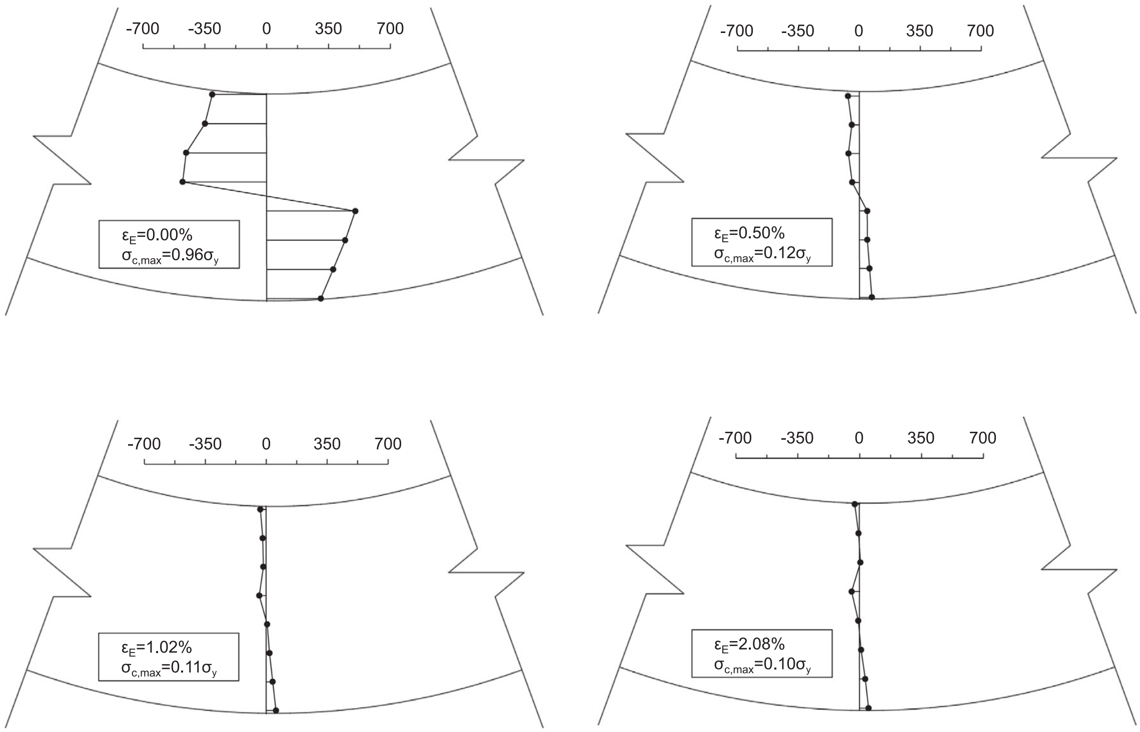

Fig. 27. Circumferential residual stress distribution [in MPa], across the thickness of the JCO-E pipe at 180-degree position, for four expansion levels. The first picture (top-left) refers to JCO pipe (no expansion).

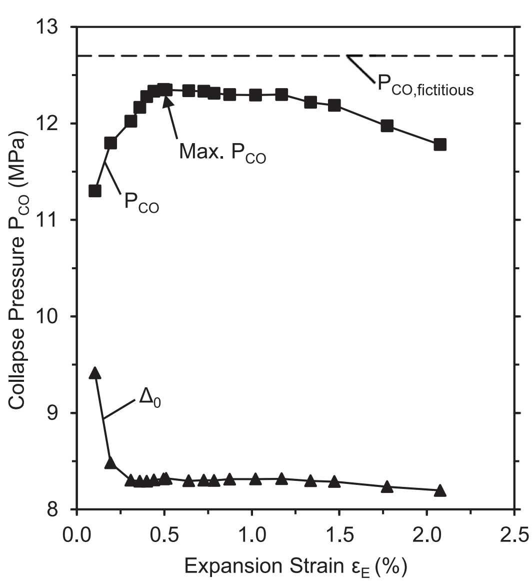

Fig. 28. Effect of expansion on collapse pressure P_{CO} and the corresponding initial ovalization Δ_0.

pressure. For expansion strain levels beyond this optimum range, the degradation of compressive strength, due to Bauschinger effect, becomes dominant leading to reduction of pipe collapse pressure. It is also found that steel plate anisotropy may not be a major factor for the value of collapse pressure. Furthermore, the numerical results show that the effect of welding process on the collapse pressure of JCO-E pipe is rather small.

As a final conclusion, the model developed in the present study constitutes a powerful and very useful numerical tool for the optimum design of offshore pipelines, capable of predicting geometrical and material properties of the JCO-E pipe product, as well as its structural response, and ultimate capacity under external pressure within a good level of accuracy.

CRediT authorship contribution statement

Konstantinos Antoniou: Writing – original draft, Software, Investigation. **Aris G. Stamou:** Writing – original draft, Software, Investigation. **Spyros A. Karamanos:** Writing – review & editing, Supervision, Funding acquisition, Conceptualization. **Christos Palagas:** Writing – review & editing, Methodology, Data curation. **Athanasios Tazedakis:** Project administration, Funding acquisition, Conceptualization. **Efthimios Dourdounis:** Writing – review & editing, Methodology, Data curation.

Declaration of competing interest

The authors declare that they have no known competing financial interests or personal relationships that could have appeared to influence the work reported in this paper.

Data availability

Data will be made available upon request.

Acknowledgments

The authors would like to thank Corinth Pipeworks S.A., Thisvi, Greece, for their financial support, their close cooperation throughout this research and their permission for publishing this paper. Many thanks also go to Dr Giannoula Chatzopoulou, now software engineer at BETA CAE Systems, Thessaloniki, Greece, for her help in the first stages of this research.

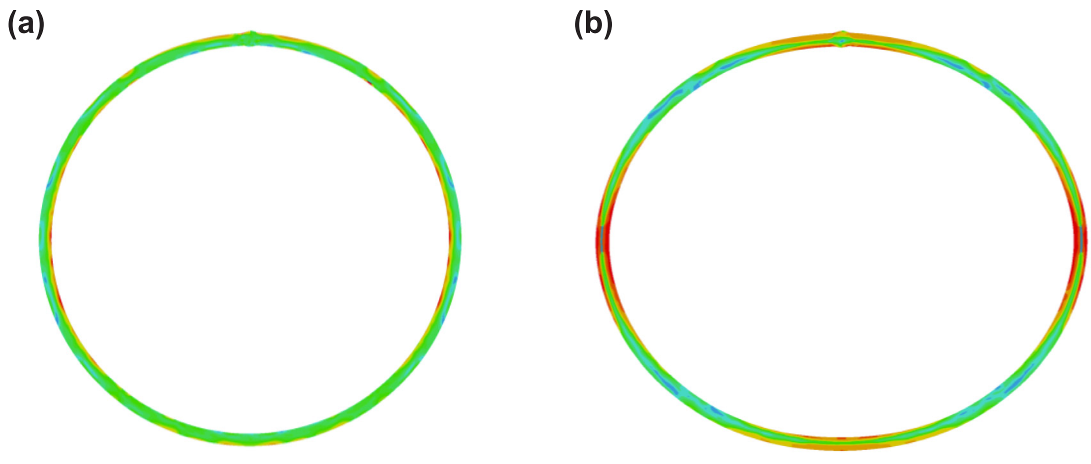

Fig. 29. Deformed cross-sectional shape of the JCO-E pipe subjected to external pressure for the case of $\varepsilon_E = 0.50\%$; (a) configuration at maximum external pressure corresponding to cross-sectional ovalization $\Delta = 1.1\%$; (b) post-buckling configuration corresponding to cross-sectional ovalization $\Delta = 8.00\%$.

Appendix. Implementation of the constitutive model

The constitutive model presented in Section 2.2 is implemented using an implicit "elastic predictor – plastic corrector" integration procedure suitable for finite element environment. The incremental problem can be stated as follows. At the start of time increment $t = t_n$, and for a given state of the known quantities $(\mathbf{s}_n, \mathbf{a}_n, \varepsilon_{q,n})$ and a given strain increment $\Delta\boldsymbol{\varepsilon}$, the new state parameters at the end of the increment $(\mathbf{s}_{n+1}, \mathbf{a}_{n+1}, \varepsilon_{q,n+1})$ are sought.

Assuming $\Delta\boldsymbol{\varepsilon} = \Delta\boldsymbol{\varepsilon}^e$, elastic prediction takes place first, excluding any plastic deformation of the material. Following a direct integration of the elasticity equation, the new state parameters at the end of the time increment t_{n+1} can be written as:

$$\begin{aligned} \mathbf{s}_{n+1} &= \mathbf{s}^{(e)} = \mathbf{s}_n + \mathbf{D}\Delta\boldsymbol{\varepsilon} \\ \mathbf{a}_{n+1} &= \mathbf{a}_n \\ \varepsilon_{q,n+1} &= \varepsilon_{q,n} \\ \varepsilon'_{q,n+1} &= \varepsilon'_{q,n} \end{aligned} \tag{27}$$

If the yield criterion in Eq. (1) is satisfied at the end of the increment $(f_{y,n+1} \le 0)$, then the above assumption of elastic prediction is valid and the time increment is elastic. Otherwise, plastic correction is necessary with the following procedure.

Substituting the plastic multiplier $\dot{\lambda}$ of Eq. (15) into Eq. (13) and integrating over the time increment using an Euler-backward integration scheme, one results in the following expression for the increment of plastic deformation:

$$\Delta\boldsymbol{\varepsilon}^p = \frac{3}{2}\frac{\Delta\varepsilon_q}{k(\varepsilon_{q,n+1})}\mathbf{N}\boldsymbol{\xi}_{n+1} \tag{28}$$

Integrating Eq. (21) over the time increment, the following expression is obtained:

$$\Delta\boldsymbol{\sigma} = \mathbf{D}\Delta\boldsymbol{\varepsilon} - \frac{3G}{k(\varepsilon_{q,n+1})}\Delta\varepsilon_q\mathbf{N}\boldsymbol{\xi}_{n+1} \tag{29}$$

which can also be written as:

$$\boldsymbol{\sigma}_{n+1} = \boldsymbol{\sigma}^{(e)} - \frac{3G}{k(\varepsilon_{q,n+1})}\Delta\varepsilon_q\mathbf{N}\boldsymbol{\xi}_{n+1} \tag{30}$$

where $\boldsymbol{\sigma}^{(e)} = \boldsymbol{\sigma}_n + \mathbf{D}\Delta\boldsymbol{\varepsilon}$ is the elastic predictor stress.

The deviatoric part of the final stress in Eq. (30) is written as:

$$\mathbf{s}_{n+1} = \mathbf{s}^{(e)} - \frac{3G}{k(\varepsilon_{q,n+1})}\Delta\varepsilon_q\mathbf{N}\boldsymbol{\xi}_{n+1} \tag{31}$$

Furthermore, integration of the nonlinear kinematic rule of Eq. (16), at the end of the time increment, results in:

$$\mathbf{a}_{n+1} = \frac{1}{1+\gamma\Delta\varepsilon_q}\left(\mathbf{a}_n + \frac{3C(\varepsilon'_{q,n+1})}{2k(\varepsilon_{q,n+1})}\Delta\varepsilon_q\mathbf{N}\boldsymbol{\xi}_{n+1}\right) \tag{32}$$

Combining Eqs. (31) and (32), the stress difference at the end of the increment $\boldsymbol{\xi}_{n+1} = \mathbf{s}_{n+1} - \mathbf{a}_{n+1}$ can be expressed as follows:

$$\boldsymbol{\xi}_{n+1} = [\mathbf{W}(\Delta\varepsilon_q)]\left(\mathbf{s}^{(e)} - \frac{1}{1+\gamma\Delta\varepsilon_q}\mathbf{a}_n\right) \tag{33}$$

where

$$[\mathbf{W}(\Delta\varepsilon_q)] = \left[\mathbf{I} + \left(\frac{3\Delta\varepsilon_q}{k(\varepsilon_{q,n+1})}\left(G + \frac{C(\varepsilon'_{q,n+1})}{2(1+\gamma\Delta\varepsilon_q)}\right)\right)\mathbf{N}\right]^{-1} \tag{34}$$

and $\mathbf{I}$ is the identity tensor. Finally, enforcing the consistency condition of flow rule, the yield condition (1) should be satisfied with the new state parameters at the end of the increment "n+1". Using Eq. (33), the yield condition (1) can be written as follows:

$$\frac{1}{2}\left\{[\mathbf{W}(\Delta\varepsilon_q)]\left(\mathbf{s}^{(e)} - \frac{1}{1+\gamma\Delta\varepsilon_q}\mathbf{a}_n\right)\right\}\cdot\left\{\mathbf{N}\left([\mathbf{W}(\Delta\varepsilon_q)]\left(\mathbf{s}^{(e)} - \frac{1}{1+\gamma\Delta\varepsilon_q}\mathbf{a}_n\right)\right)\right\} = \frac{k^2(\varepsilon_{q,n+1})}{3} \tag{35}$$

The above equation is solved in terms of the equivalent plastic strain increment $\Delta\varepsilon_q$ using the secant iteration method:

$$\Delta\varepsilon_{q(i+1)} = \Delta\varepsilon_{q(i)} - f_y(\Delta\varepsilon_{q(i)})\frac{\Delta\varepsilon_{q(i)} - \Delta\varepsilon_{q(i-1)}}{f_y(\Delta\varepsilon_{q(i)}) - f_y(\Delta\varepsilon_{q(i-1)})} \tag{36}$$

The following two initial values are used to initiate this iterative process: (a) zero value for $\Delta\varepsilon_{q(-1)}$ and (b) $\Delta\varepsilon_{q(0)} = \frac{\sigma_v^{(e)} - k(0)}{3G+H}$ corresponding to the solution of an isotropic plasticity model with kinematic hardening., where $\boldsymbol{\sigma}_v^{(e)}$ denotes the von Mises stress at the initial stage (e) and H is the hardening modulus. Substituting the equivalent plastic strain increment $\Delta\varepsilon_q$ into Eq. (31) and (32), the new state of stresses $\mathbf{s}_{n+1}$ and $\mathbf{a}_{n+1}$ at the end of the increment are calculated.

References

[1] Peter R. Stark, David S. McKeehan, Hydrostatic Collapse Research in Support of the Oman India Gas Pipeline, Offshore Technology Conference, Houston, Texas, 1995.

[2] D. DeGeer, C. Timms, V. Lobanov, Blue stream collapse test program, in: ASME 24th International Conference on Offshore Mechanics and Arctic Engineering, Vol. 3, 2005, pp. 499–507.

[3] Chris M.J. Timms, Duane D. DeGeer, Mohamed R. Chebaro, Y. Tsuru, Compressive strain limits of large diameter X80 UOE linepipe, in: Nineteenth International Offshore and Polar Engineering Conference, Osaka, Japan, 2009.

[4] S. Kyriakides, E. Corona, F.J. Fischer, On the Effect of the UOE Manufacturing Process on the Collapse Pressure of Long Tubes, Offshore Technology Conference, Houston, Texas, 1991.

[5] M.D. Herynk, S. Kyriakides, A. Onoufriou, H.D. Yun, Effects of the UOE/UOC pipe manufacturing processes on pipe collapse pressure, Int. J. Mech. Sci. 49 (5) (2007) 533–553.

[6] R.G. Toscano, J. Raffo, L. Mantovano, M. Fritz, R.C. Silva, On the Influence of the UOE Process on Collapse and Collapse Propagation Pressure of Steel Deep-Water Pipelines under External Pressure, Offshore Technology Conference, Houston, Texas, 2007.
[7] G. Chatzopoulou, S.A. Karamanos, G.E. Varelis, Finite element analysis of UOE manufacturing process and its effect on mechanical behavior of offshore pipes, Int. J. Solids Struct. 83 (2016) 13–27.
[8] K. Antoniou, G. Chatzopoulou, S.A. Karamanos, A. Tazedakis, C. Palagas, E. Dourdounis, Numerical simulation of JCO-E pipe manufacturing process and its effect on the external pressure capacity of the pipe, ASME J. Offshore Mech. Arct. Eng. 141 (1) (2019).
[9] J.D. Chandel, N.L. Singh, Formation of X-120 M line pipe through $J-C-O-E$ technique, Engineering 3 (2011) 400–410.
[10] L.F. Fan, J.X. Yan, Y. Gao, J.B. Yun, Research on deformation characteristics of JCOE forming in large diameter welding pipe, Adv. Manuf. 4 (2016) 268–277.
[11] Y. Gao, Q. Li, L. Xiao, Numerical Simulation of JCO/JCOE Pipe Forming, World Congress on Computer Science and Information Engineering, Los Angeles, CA, USA, 2009.
[12] T. Kathayat, R. Goyal, J. Shant, Collapse Behavior of As-Fabricated & Thermal Aged JCOE Line Pipe - Experimental Study By External Pressure Ring Collapse Testing and FE Analysis, Offshore Technology Conference, Asia, Kuala Lumpur, 2014.
[13] V.R. Krishnan, D.A. Baker, Enhanced collapse resistance of compressed steel pipes, in: Proceedings of the 33rd International Conference on Ocean, Offshore and Arctic Engineering, San Francisco, California, USA, 2014.
[14] T. Reichel, V. Pavlyk, J. Beissel, S. Kyriakides, W.Y. Jang, New Impander Technology for Improved Collapse Resistance of Large Diameter Pipe for Deepwater Applications, Offshore Technology Conference, Houston, Texas, 2011.
[15] P.J. Armstrong, C.O. Frederick, A mathematical representation of the multiaxial bauschinger effect, CEGB Report No. RD/B/N 731, 1966.
[16] M. Kojic, N. Grujovic, R. Slavkovic, M. Zivkovic, A general orthotropic von mises plasticity material model with mixed hardening: Model definition and implicit stress integration procedure, J. Appl. Mech. 63 (2) (1996) 376–382.
[17] R. Hill, The Mathematical Theory of Plasticity, Oxford University Press, London, 1950.
[18] J. Lemaitre, J. Chaboche, Mechanics of Solid Materials, Cambridge University Press, Cambridge, 1990.
[19] DS Simulia Corp., Abaqus Analysis User's Guide, Version 6.14, RI, USA.
[20] Y. Ren, Investigation of residual stresses in X65 narrow-gap pipe girth welds, (Ph.D. Thesis), Department of Mechanical, Aerospace and Civil Engineering, Brunel University London, 2018.
[21] ISO/TR 17671-1, Welding – Recommendations for Welding of Metallic Materials, International Standardization Organization (ISO), Geneva, Switzerland, 2002.
[22] J. Goldak, A. Chakravarti, M. Bibby, A new finite element model for welding heat sources, Metall. Trans. B 15 (1984) 229–305.
[23] A.H. Yaghi, D.W.J. Tanner, T.H. Hyde, A.A. Becker, W. Sun, Finite element thermal analysis of the fusion welding of a P92 steel pipe, Mech. Sci. 3 (2012) 33–42.
[24] Y. Bai, Q. Bai, Subsea Pipelines and Risers, Elsevier, 2005.
[25] I.W. Bang, Y.P. Son, K.H. Oh, Y.P. Kim, W.S. Kim, Numerical simulation of sleeve repair welding of in-service gas pipelines, Weld. J. 81 (2002) 273–282.
[26] T. Horn, Cyclic plastic deformation and welding simulation, (Doctoral Thesis), Faculty of Materials Science, Delft University of Technology Press, 2003.
[27] S.A. Karamanos, Structural Mechanics and Design of Metal Pipes, A Systematic Approach for Onshore and Offshore Pipelines, first ed., Elsevier, 2022.
[28] S. Kyriakides, E. Corona, Mechanics of Offshore Pipelines, Buckling and Collapse, Vol. 1, Elsevier, 2007.
[29] Stahl-Eisen-Prüfblätter, Testing and Documentation Guideline for the Experimental Determination of Mechanical Properties of Steel Sheets for CAE-Calculations, SEP 1240, Research Association for Steel Application, Wuppertal/Germany, 2006.
[30] ISO 6892-1, Metallic Materials - Tensile Testing - Part 1: Method of Test at Room Temperature, International Standardization Organization (ISO), Geneva, Switzerland, 2016.
[31] M.R. Nezamdost, M.R. Nekouie Esfahani, S.H. Hashemi, S.A. Mirbozorgi, Investigation of temperature and residual stresses field of submerged arc welding by finite element method and experiments, Int. J. Adv. Manuf. Technol. 87 (2016) 615–624.
[32] Submarine Pipeline Systems, STANDARD DNV-ST-F101, Høvik, Norway, 2021.
[33] American Petroleum Institute, Design, Construction, Operation and Maintenance of Offshore Hydrocarbon Pipelines (Limit State Design), API RP 1111, 1999.